5105-149
Solar Thermal Power Systems Project
Parabolic Dish Systems Development

Dish-Stirling Module Performance As Evaluated from Tests of Various Test Bed Concentrator/ Stirling Engine Configurations

M. K. Selcuk

June 15, 1985

Prepared for
U.S. Department of Energy
Through an Agreement with
National Aeronautics and Space Administration
by

JPL

Jet Propulsion Laboratory
California Institute of Technology
Pasadena, California

JPL D-2637

5105-149
Solar Thermal Power Systems Project
Parabolic Dish Systems Development

Dish-Stirling Module Performance As Evaluated from Tests of Various Test Bed Concentrator/ Stirling Engine Configurations

M. K. Selcuk

June 15, 1985

Prepared for
U.S. Department of Energy
Through an Agreement with
National Aeronautics and Space Administration
by

JPL

Jet Propulsion Laboratory
California Institute of Technology
Pasadena, California

JPL D-2637

Prepared by the Jet Propulsion Laboratory, California Institute of Technology, for the U.S. Department of Energy through an agreement with the National Aeronautics and Space Administration.

The JPL Solar Thermal Power Systems Project is sponsored by the U.S. Department of Energy and is part of the Solar Thermal Program to develop low-cost solar thermal and electric power plants.

ABSTRACT

During the past several years, many tests of the dish-Stirling module comprising either of two test bed concentrators, one of several cavity receivers, and one of three United Stirling of Sweden (USAB) 4-95 Stirling engines in original or modified configuration, together with various sets of auxiliary and peripheral equipment have been tested at the Parabolic Dish Test Site located at the Jet Propulsion Laboratory (JPL) Edwards Test Station.

The test data resulting from these tests had accumulated without a sustained and concerted effort toward their further reduction by JPL because USAB was granted primary responsibility for conducting the tests.

This report presents the results obtained by analysis of what have been judged to be the most significant of these sets of test data. Considerable effort was made at the outset of this task to review all the available data sets and to select only those that exhibited excellent to good module performance for the more promising configurations under favorable test conditions. These data are considered to be reflective of the progress made during the test effort.

The results presented in this report reflect the generally superior capabilities of dish-Stirling solar thermal electric power modules.

ACKNOWLEDGMENTS

The author wishes to thank the following people for their contributions to this report: H. G. Nelving, W. H. Percival, and D. Wells of United Stirling and M. E. Alper, F. R. Livingston, J. W. Lucas, P. L. Panda, M. Rice, and J. W. Stearns of the Jet Propulsion Laboratory.

The work described herein was conducted by the Jet Propulsion Laboratory, California Institute of Technology, for the U.S. Department of Energy through an agreement with the National Aeronautics and Space Administration (NASA Task RE-152, Amendment 327; DOE/ALO/NASA Interagency Agreement No. DE-AM04-80AL13137).

PREFACE

The appendixes referred to in this report are proprietary and have been designated for assigned Government use on a need-to-know basis only. Therefore, they are not included as part of this publication.

CONTENTS

SECTION I

INTRODUCTION

A. BACKGROUND

A dish-Stirling test program was conducted by United Stirling of Sweden (USAB) at the Jet Propulsion Laboratory (JPL) Parabolic Dish Test Site (PDTS). JPL provided support in operating and maintaining the test facility during the course of the tests. The reduced test data, as recorded by the PDTS data acquisition system, were available for independent JPL studies. The author of this report analyzed the test results as they became available during and after test completion. The author was essentially isolated from the planning and execution of the testing, and therefore relied solely on the available recorded data for his analyses.

B. OBJECTIVE

The objective of the study whose results are reported herein was to independently examine the test data to assess (1) module performance and (2) developmental potential of the module.

C. SCOPE AND CAVEATS

The tests that were run primarily provided operating experience on engine/receiver combinations in the test environment involving operation with solar energy. Emphasis was placed on full-power operation. For these reasons, the data base for part-load power is very limited. Within the limitations of this data base, the effort reported here sought to examine factors such as part-load performance and to provide insights regarding trends in the performances of the variant systems.

SECTION II

DESCRIPTION OF RECEIVER TYPES

Because a hybrid Stirling engine heater head configuration having a potential capability of operation both with fossil fuel and the sun as energy sources had already been tested, the new USAB receiver design series was identified as the Experimental Solar-Only Receiver (ESOR) to distinguish it from the hybrid receiver.

Several variations of the solar-only receiver were tested under the cognizance of USAB engineers and technicians. JPL provided the facility but did not lead the preplanning nor direct the performance of the experiments. Prior to this report, no formal publication or interpretation of the data had been attempted, although some informal reports were prepared in 1982 and 1983. Copies of these reports are presented in Appendix B of this report.

The generic receiver enclosure discussed here consists of an aperture cone and a housing that forms the receiver cavity and protects the heater head tubing from wind and other environmental effects.

Each particular receiver configuration will be described briefly prior to discussing the performance of the corresponding experiments and interpretation of the resulting test data.

A. ESOR-I

"Experimental Solar-Only Receiver, Model I" (ESOR-I) employed, essentially unmodified, the heater head that was used when the 4-95 engine was operated with a combustor (Figure 2-1). The tube configuration was originally selected for optimum heat transfer from combustion products to the working fluid inside the tubes. Therefore, the diameter of the tube cone formed by the heater tubes is not optimized for solar operation. There are fins on the rear tubes that are not exposed to sunlight. These tubes were originally introduced to enhance the convective heat transfer when the combustor was used; with the solar-only receiver, these finned tubes played a detrimental role. Due to an improperly concentrated flux pattern on the tube bundle and non-optimized tube coil dimensions, spillage of some concentrated flux onto the receiver inner walls was unavoidable, and ESOR-I yielded lower efficiencies than had been expected.

In view of the poor performance of ESOR-I, new generations of receivers were designed and tested: ESOR-IIA, ESOR-IIB, ESOR-III, and ESOR-IV.

B. ESOR-IIA

The ESOR-IIA heater head is the first heater tube configuration specifically designed for use with a solar concentrator. The rear tube fins were eliminated, and the front tube cone diameter was increased to intercept

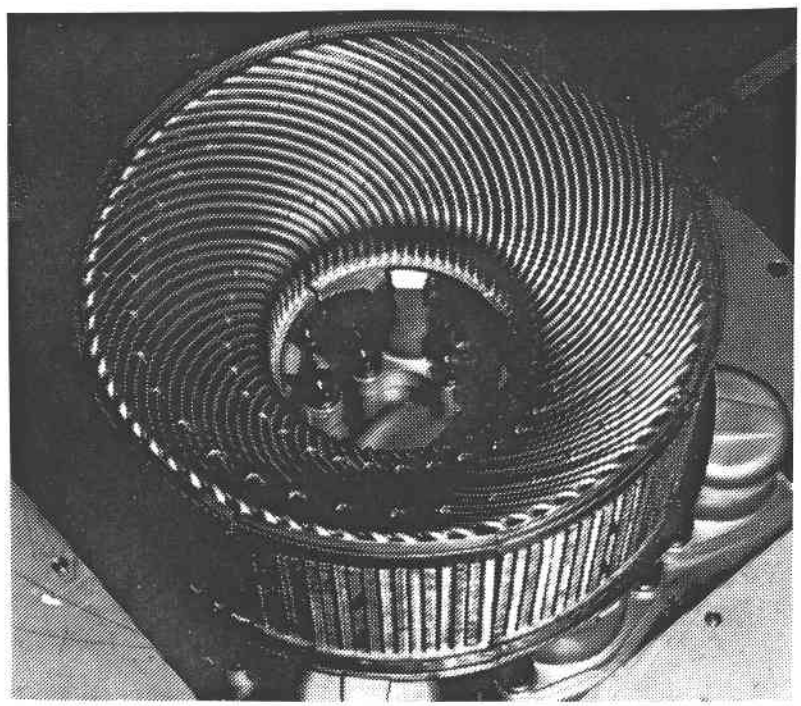

Figure 2-1. ESOR-I Heater Head

virtually all of the concentrated flux entering the receiver aperture. Front and rear tubes are joined in a common circular manifold, cf. Figure 2-2.

C. ESOR-IIB

The configuration of ESOR-IIB is very similar to ESOR-IIA but, as seen in Figure 2-3, does not have a peripheral manifold.

D. ESOR-III

The design of ESOR-III is based upon experience gained with earlier designs. Its configuration is very similar to that of ESOR-IIB. The tubes have been shaped to form a coil at the top of the cone. The space between the front and rear portions of the tubes is filled with insulation. Figure 2-4 is a photograph of the ESOR-III heater head.

E. ESOR-IV

ESOR-IV is the latest design evolved from several years of experience with engine and receiver development. The tube coil configuration is similar to that of ESOR-III. The major difference is the absence of the tube manifold at the regenerator end of the heater tube assembly. Unlike the earlier heater tube assemblies, the regenerator ends of tubes are directly connected onto the regenerator head. Thus, in the case of the ESOR-IV heater tube assembly, tube

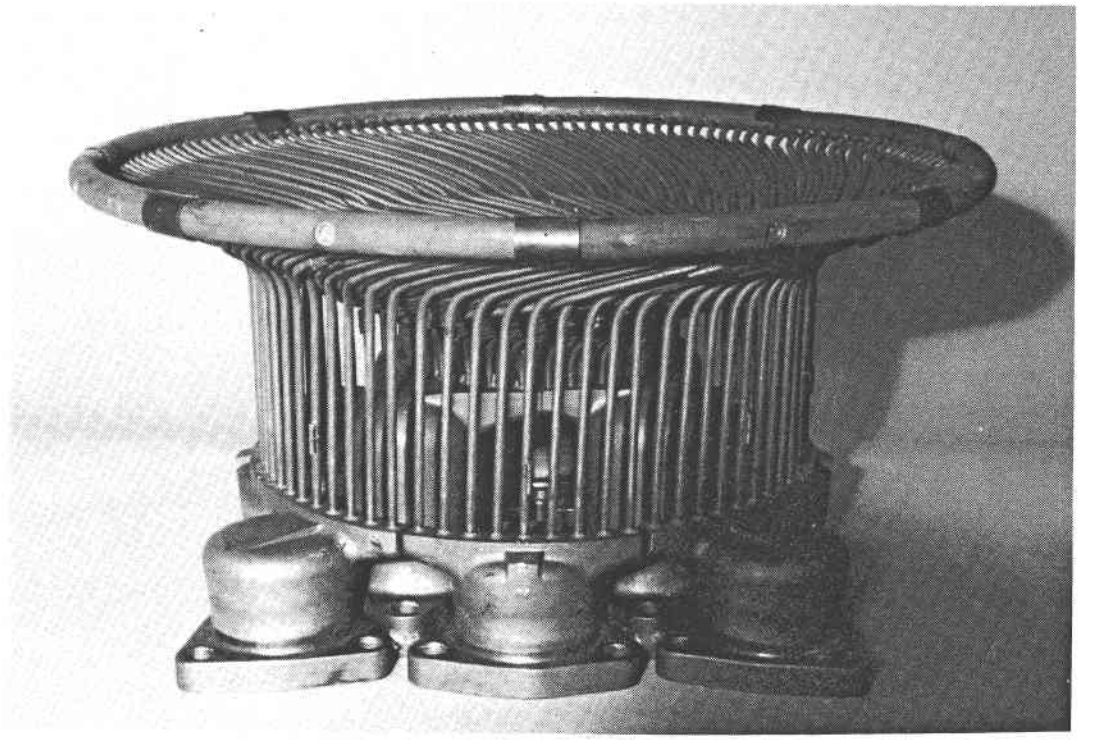

Figure 2-2. ESOR-IIA Heater Head

Figure 2-3. ESOR-IIB Heater Head

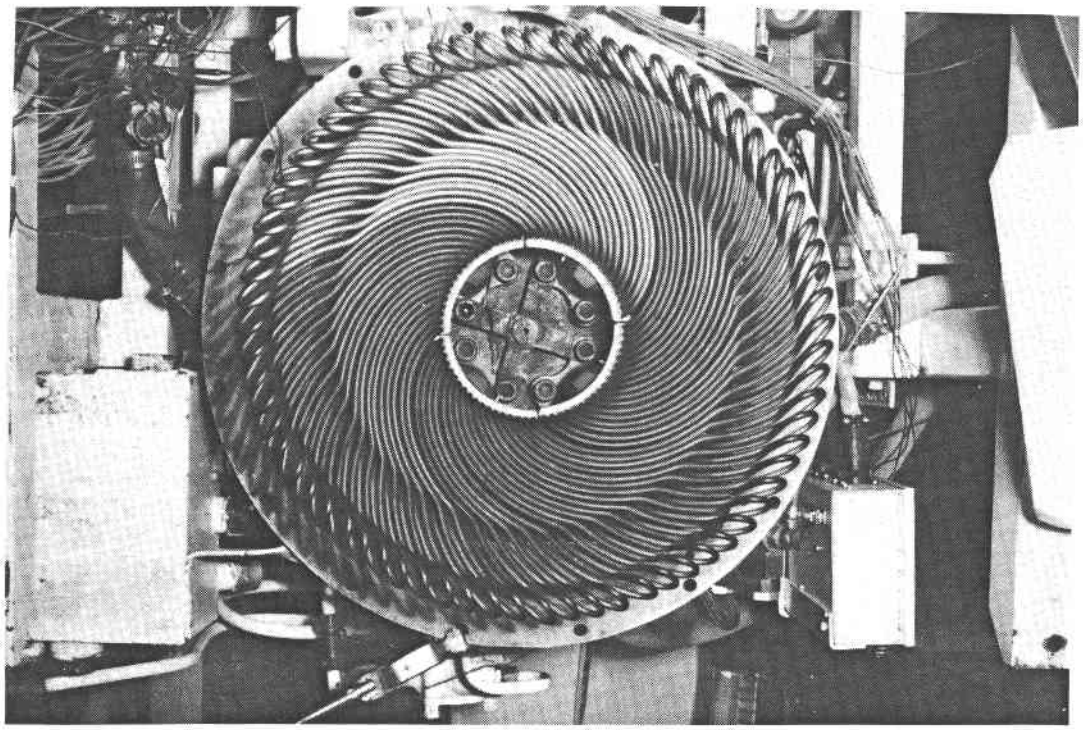

Figure 2-4. ESOR-III Heater Head

length is shortened, dead volume is reduced, and better flow distribution is obtained. Figure 2-5 is a photograph of the ESOR-IV heater head.

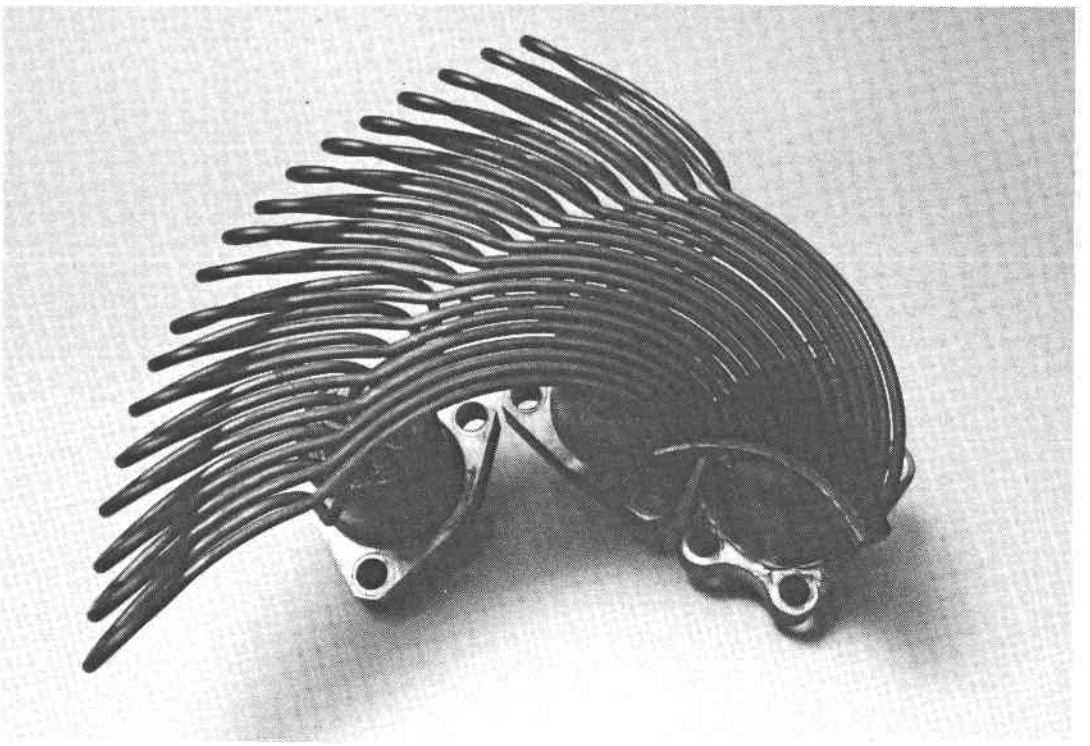

Figure 2-5. ESOR-IV Heater Head

SECTION III

CHRONOLOGY OF TESTS CONDUCTED

Under an agreement between JPL and USAB, a total of 266 ESOR tests were performed at the PDTS starting in January 1982.

The full list of tests run is presented in Appendix A. A summary list of the test groups with appropriate references to the corresponding internal documents issued during 1982 is presented in Table 3-1. All tests were performed on the test bed concentrators (TBCs) located at the PDTS.

The results obtained from selected tests run during 1983 and January 1984 are presented for the first time in this report.

ESOR-I tests were initiated during January 1982. Test results are summarized in Appendix B-I. Because results from this series of tests were unsatisfactory, a new series of receiver tests was started after February 1982.

The first series of tests on ESOR-IIA and ESOR-IIB was run during February and March, 1982. Results from selected tests conducted during that time period are summarized and discussed in Appendixes B-I and B-II.

The second series of tests of ESOR-IIA and ESOR-IIB conducted by USAB commenced on May 21, 1982, and continued until July 20, 1982. The purpose of this test series was to evaluate these experimental receivers at various optimum positions with respect to the concentrator focal plane and to determine an optimum position for each receiver with respect to the focal plane. Capability to adjust the power conversion unit (PCU) position along the Z-axis of the concentrator was provided to satisfy this requirement. From this testing, USAB designed a new receiver having better performance than either ESOR-IIA or ESOR-IIB.

By mid-May 1982, the mirrors of a PDTS test bed concentrator (namely, TBC-2) had been realigned to a focal plane 22.9 cm (9 in.) inside the face of the PCU mounting ring. The "A" mirrors (i.e., mirror panels at the central region of the dish) were cross-focused to leave a dark inner circle of approximately 10 cm (4 in.) in diameter at the focal plane and, thus, to avoid impingement of the concentrated solar flux upon the Stirling receiver center plug.

The receiver ESOR-IIA was installed on the Stirling engine/alternator and mounted on TBC-2 during the week of May 17, 1982. A new microprocessor controller was integrated into the system. System operation commenced on May 21, 1982. Water-cooled shutters at the mounting ring were modified to allow their opening to a wider limit. The engine cooling system, supplied by JPL, also supplied water to the water-cooled aperture plates.

Testing commenced with 50% of the mirrors exposed and then continued with 80%, exposed. Receiver position was varied to determine its optimum location along the Z-axis of the dish. During this optimization process, on May 27, a helium leak developed in one of the heater head tubes. Examination after demounting from TBC-2 showed the leak to be through a crack along the

Table 3-1. Summary of ESOR Tests[a]

Test Run No.	Receiver Type	Working Fluid	Test Period	Report Issued	Appendix Reference
119-124	ESOR I	Helium	Jan 17, 1982		
125-138	ESOR IIA	Helium	Feb 2, 26	3411-82-046	B-I
139-150	ESOR IIB	Helium	Mar 4-15, 31	3411-82-075	B-II
157-160	ESOR IIA	Helium	May 21-27	3410-82-361	B-III
161-171	ESOR IIB	Helium	Jun 2-17	3410-82-361	B-III
172-176	ESOR IIB	Helium	Jun 21-23	3411-82-110	B-IV
177-183	ESOR IIA	Helium	Jul 1-13	3411-82-114	B-V
184-185	ESOR IIA	Hydrogen	Jul 14-15	3411-82-116	B-VI
186-187	ESOR IIA	Helium	Jul 16-20	3411-82-114	B-V
188-200	ESOR IIA	Helium	Sept 17-Oct 11	3410-82-469	B-VII
201-216	ESOR IIB	Helium	Oct 18-Dec 17		
217-218	ESOR IIB	Helium	Jan 17-18, 1983	(All runs during 1983 and 1984 are reviewed for the first time by JPL in this report.)	
219-228	ESOR IIA	Helium	Feb 1-24		
229-235	ESOR III	Helium	Mar 8-31		
236-239	ESOR IIA	Helium	Apr 4-8		
240-247	ESOR III	Helium	Apr 7-May 2		
248-268	ESOR IIA	Helium	May 9-Jun 3		
269-283	ESOR III	Helium	Jun 10-Jul 5		
284-305	ESOR IIA, ESOR III	Helium	Jul 6-27[a]		
306-314	ESOR III	Hydrogen	Jul 28-Aug 11		
315-316	ESOR III (H_2), ESOR IIA	H_2 & He	Aug 12		
317-356	ESOR III (H_2), ESOR IIA	H_2 & He	Aug 18-Oct 13[a]		
357-359	ESOR IV	Hydrogen	Oct 21-24		
360-362	ESOR III	Hydrogen	Oct 27-Nov 9		
363-365	ESOR IV	Hydrogen	Nov 14-15		
362-364	ESOR III	Hydrogen	Nov 9-15		
366-375	ESOR III	Hydrogen	Nov 17-Dec 8		
376-378	ESOR IV	Hydrogen	Dec 19-20		
384-385	ESOR IV	Helium	Jan 23-25, 1984		

[a]Simultaneous tests of two engines, each installed on one of the two TBCs, were run during this period.

seam of the tube. Rolled and welded tubing rather than seamless tubing had been used with this receiver. Repair materials were sent from Sweden. The quadrant was carried to Solar Turbines, Inc., in San Diego on June 3, where it was repaired by brazing; the unit was returned to JPL on June 7. Results from this series of tests are presented in Appendix B-III.

The experimental receiver ESOR-IIB was installed on the Stirling engine/alternator assembly, and the system was mounted on TBC-2 on June 2, 1982. Testing commenced with 80% of the mirrors uncovered and continued through June 7. On June 8, 1982, the system began operation with 100% mirrors. From that date until June 16, the Z-axis position of the engine was varied over its full range. The search for optimum heater head position was continued until June 17. On June 18, mirrors were cleaned and the engine was recharged with hydrogen as the working fluid. From June 21 to June 23, the module was run from sunrise to sunset. The engine was programmed over a full range of temperatures and pressures during these tests with hydrogen as the working fluid. Test results have been presented and discussed in Appendixes B-III and B-IV. These tests were completed, and reinstallation of ESOR-IIA began on July 1, 1982.

During July 1982, tests continued with ESOR-IIA located at various Z-axis positions. Except for two days (July 14 and 15) when tests were run with hydrogen as the working fluid, all tests were conducted with helium as the working fluid. Test results have been summarized and discussed and are presented in Appendixes B-V and B-VI. Testing with ESOR-IIA was temporarily suspended on July 20, 1982. ESOR-IIA tests with helium were resumed in September; some of these results are presented in Appendix B-VII. Tests with ESOR-IIA continued during 1983. Tests were performed with helium and hydrogen at various Z-axis positions. Tests were also run with and without a quartz window behind the aperture and with a radiator at the focal plane.

Testing with ESOR-III commenced on March 8, 1983. Helium and hydrogen were used as the working fluids. Testing continued throughout 1983. Tests were conducted with the heater head located at various Z-axis positions. In an effort to reduce the convective losses over the heater head tubes, ESOR-III was also tested with a quartz window installed behind the aperture plane.

A limited number of ESOR-IV tests using hydrogen as the working fluid were run during the months of October, November, and December of 1983. Only two significant runs from the most recent series of tests (performed during January 1984) employed helium as the working fluid.

SECTION IV

GENERAL REMARKS REGARDING THE TESTS

It is emphasized here that the solar energy flux into the receiver aperture was, prior to Run No. 217 on January 17, 1983, calculated by the on-line data system as being 80 kWt for a direct normal insolation of 1000 W/m^2; beginning with Run No. 217, the flux into the receiver aperture for the same 1000 W/m^2 was calculated as 75 kWt. As calibration of TBC-1 and -2 progressed after Run No. 217 and as certain errors in the calibrating instruments themselves were eliminated, it became clear that an assumption of 75 kWt into a 20-cm (8-in.)-diameter receiver aperture at a direct normal insolation of 1000 W/m^2 better represented the insolation collection capability of the TBCs under usual conditions of mirror cleanliness than did 80 kWt at the same insolation level.

In those cases where data collected in tests prior to January 17, 1983, are presented in figures in the body of this report, the energy flux through the aperture has been corrected so as to correspond to 75 kWt at a direct normal insolation of 1000 W/m^2. The data presented in the appendixes have not been corrected to 75 kWt. They are still based on 80 kWt.

In reassessing any data previously reported but included in the body of this report, it has been possible to exercise additional care in eliminating obviously inconsistent data that were recorded under unsteady operating conditions and to classify the consistent data in more precise ways, e.g., by mean heater head gas temperature, receiver aperture position, presence or absence of a receiver window, radiator cross-sectional area exposed to cooling air flow, etc.

SECTION V

SCREENING OF TEST DATA AND SELECTION OF TESTS FOR EVALUATION

Since the last previous internal report analyzing Stirling test data was issued on December 20, 1982, almost 200 tests have been performed on two different USAB 4-95 engines using several different heater heads. Tests were performed with heater heads ESOR-IIA, ESOR-IIB, ESOR-III and ESOR-IV. Both hydrogen and helium were used as working fluids. A quartz window designed to reduce the convection losses was also tested. Most of the tests were run using a ground-mounted radiator; however, some tests were run using an oversized, focal-plane-mounted radiator.

A full list of tests run is presented in Appendix A. Run number, date, type of receiver, concentrator mirror coverage, the position of the aperture plane with respect to focal plane, and working fluid are shown. Run Nos. 118 through 200 were selectively evaluated; these results are presented in Appendix B as follows:

(1) Appendix B-I: ESOR-I, ESOR-IA, and ESOR-IIB receiver test data are evaluated and summarized. Data from Run Nos. 124, 128, 133, 138, 139, and 142 were used. The working fluid was helium.

(2) Appendix B-II: ESOR-IIB receiver was used. Tests were run on March 30 and 31 with hydrogen as the working fluid. All other tests reported in this appendix used helium.

(3) Appendix B-III: ESOR-IIA and ESOR-IIB were tested. Results from tests run on May 24 until June 17, 1982, are examined. The working fluid was helium.

(4) Appendix B-IV: Test data on ESOR-IIB using hydrogen as working fluid are presented, showing power output versus receiver heat input.

(5) Appendix B-V: Most of the test data acquired during July 1982 is presented. Tests performed on July 14 and 15, 1982, were examined in another report. Tests were run from July 1 through July 20 using helium as the working fluid. Power output versus receiver input relations are shown.

(6) Appendix B-VI: ESOR-IIA was tested using hydrogen as the working fluid on July 14 and 15, 1982. Test results were summarized and power output versus heat input relations are shown.

(7) Appendix B-VII: Tests with ESOR-IIA run during September and October 1982 with helium as the working fluid are examined. Results were compared with the test data of July 14 and 15, which were discussed in Appendix B-VI.

(8) Appendix B-VIII: Partial load performance of the Stirling module based on January through May 1982 data is discussed. ESOR-I, ESOR-IIA, and ESOR-IIB data are examined.

Additional data acquired during 1982, from October 18 until December 17, were screened and tabulated, but a corresponding internal report was not issued.

Two runs among these tests, Run Nos. 210 and 212, performed on November 24 and December 2, 1982, have been recently reexamined and are presented in the body of this report. Some earlier tests results, selected from Run Nos. 180 through 200,were also reexamined. Thus, test Run Nos. 180 through 385 were grouped according to the heater head type, working fluid operating temperature, and other special features. Based on those criteria, the following test categories were identified:

(1) ESOR-IIA Tests, helium, full radiator, no window.
(2) ESOR-IIB Tests, helium, full radiator, no window.
(3) ESOR-IIA Tests, helium, full radiator, with window.
(4) ESOR-IIA Tests, helium, partial radiator, no window.
(5) ESOR-III Tests, hydrogen, full radiator, no window.
(6) ESOR-III Tests, helium, full radiator, no window.
(7) ESOR-IV Tests, hydrogen, full radiator, no window.
(8) ESOR-IV Tests, helium, full radiator, no window.

These tests are listed with corresponding testing conditions and operating temperatures in Table 5-1.

Table 5-1. ESOR Test Categories Examined in this Report

Category No.	Figure No.	TBC No.	Run No.	ESOR No.	Working Fluid	Conditions	Mean Heater Head Temperature, °C
1	6-1	2	186,199,200	IIA	Helium	No window	650
	6-2		183,196,197,258,260,263			Full radiator	650
	6-3		182,195				650
	6-4		180,181,190,192				650
	6-5		178,179				650
	6-6		177				650
	6-7		183,196,197,198,260,261				650
	6-8		183,196,197,258,260,263				650
	6-9		183,197,257,258,260,261, 263,264				700
	6-10	1	288,289,318				600
	6-11		289,318				650
	6-12		289,318				700
2	6-13	2	210,212	IIB	Helium	No window Full radiator	700
3	6-14	2	250,525,253,265,266	IIA	Helium	With window	700
	6-15		250,252,253,255,265,266, 268			Full radiator	700

Continued

Table 5-1. ESOR Test Categories Examined in this Report (Cont'd)

Category No.	Figure No.	TBC No.	Run No.	ESOR No.	Working Fluid	Conditions	Mean Heater Head Temperature, °C
4	6-16	1	324,326,329,331,332,334, 336,338	IIA	Helium	No window Variable radiator	700
5	6-17	2	330	III	Hydrogen	No window Full radiator	700
6	6-18	2	240,245,272,273,274,277	III	Helium	No window	600
	6-19	2	271,276,277			Full radiator	650
	6-20	2	277				700
7	6-21	2	363	IV	Hydrogen	No window	600
	6-22		363			Full radiator	650
8	6-23	2	379,381	IV	Helium	No window	550
	6-24		379,381,384,385			Full radiator	600
	6-25		381,384,385				650

SECTION VI

DISCUSSION OF TEST RESULTS

Tests were categorized into 8 groups, as given in the preceding table. Each category is discussed in detail in this section. As with most assessments made in this report, perceptible distinctions were not provided by any one test. Therefore, all pertinent data were considered before definite trends were inferred.

A. ESOR-IIA WITH HELIUM, FULL RADIATOR, AND NO WINDOW (CATEGORY NO. 1)

Figures 6-1 through 6-9 (primarily Figures 6-7 through 6-9) and their corresponding tables show the effect of varying average working gas temperature in the heater heads. As with virtually all the data reported here, the range of heat power inputs through the receiver aperture was insufficient to establish an accurate value for dP_{out}/dQ_{in}, i.e., the rate of change of electrical power out (P_{out}) with thermal power in (Q_{in}). Nevertheless, it is possible to recognize by comparison of these figures that no appreciable improvement in efficiency occurred between 600 and 650°C but that an improvement in output power of about 1.5 kWe occurred at 60 kWt heat power input between 600 and 700°C. Note, however, that the standard deviation for the data taken at 600°C is 0.85 kWe while that for data taken at 700°C is 0.60 kWe; thus, the 1.5 kWe difference noted above is only marginally significant.

B. ADDITIONAL TESTS ON ESOR-IIA WITH HELIUM, FULL RADIATOR, AND NO WINDOW (CATEGORY NO. 1)

At a much later time during the parabolic dish Stirling test program, a TBC-1/ESOR-IIA/USAB 4-95 (helium) configuration was tested at 600, 650, and 700°C; the results are presented in Figures 6-10, 6-11, and 6-12 and corresponding tables, respectively. Again, the values of dP_{out}/dQ_{in} are unreliable. It must be noted that the configuration parameters presented in the data report corresponding to test run No. 318 were inconsistent: mirror exposure was noted to be 80% on the computer printout; however, fragmentary log notes indicated 100% exposure at the insolation levels recorded. Comparison of Figures 6-10, 6-11, and 6-12 with corresponding Figures 6-7, 6-8, and 6-9 show good agreement. It is therefore concluded that the performances of TBC-1 and -2 are nearly identical. However, Figures 6-10 and 6-12 reveal a 1.3 kWe improvement in P_{out} at 650°C over that at 600°C for Q_{in} = 60 kWt and no more than 0.3 kWe improvement in P_{out} at 650°C over that at 700°C for Q_{in} = 60 kWt! One can derive some slight assurance by noting that the increase in P_{out} at Q_{in} = 60 kWt (when average heater head gas temperature is raised from 600 to 700°C) is (to the accuracy of the data) the same, whether determined by comparing Figures 6-7 and 6-9 or Figures 6-10 and 6-12. As in the earlier comparison, the standard deviations of the data sets corresponding to Figures 6-7 and 6-9 are too large to allow, on the basis of this evidence alone, the firm conclusion that performance of the power conversion assembly (receiver plus PCU) increases with average gas temperature within the heater heads.

Notes pertaining to data tables for Figures 6-1 through 6-25:

- The first value following NDEG,SIGFAC is the degree of the approximating polynomial.
- The second value following NDEG,SIGFAC is the significance factor associated with the fit.
- Let a = the third value on the next line ("P=") and b = the fourth value, then electrical power output (P_{out}) is equal to $a + bQ_{in}$, where Q_{in} represents heat input.
- Test run nos. are under column heading "RUN".
- Values for Q_{in} experimental are under column heading "X".
- Rounded values for P_{out} experimental are under column heading "Y".
- Values (calculated by formula) for P_{out} are under column heading "YFIT".
- Values under column heading "R" are determined by the relation R + YFIT = Y; however, note that Y as tabulated here has been rounded, so the equality is sometimes inexact. These values include alternator losses but not parasitics for a 20-cm-diameter receiver aperture.
- Electrical power output is in kilowatts-electric.
- Heat power input is in kilowatts-thermal.

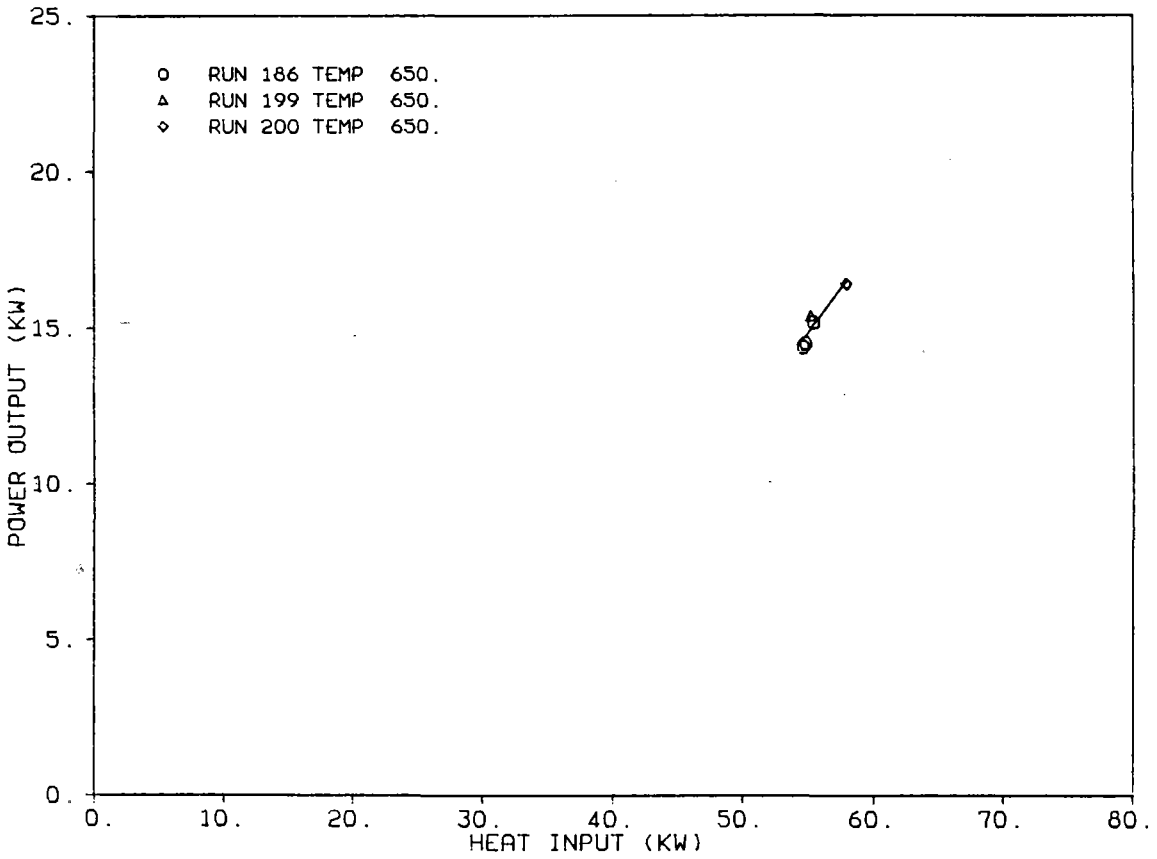

NDEG,SIGFAC 1 .3112

P = .00000000 1.00000000 -16.71628857 .57348486

RUN	X	Y	YFIT	R	
186	54.600	14.4	14.596	-.216	TBC-2
186	54.800	14.5	14.711	-.221	ESOR-IIA, He, full
186	55.400	15.2	15.055	.105	radiator, no window
199	55.200	15.4	14.940	.420	T = 650°C
200	57.900	16.4	16.488	-.088	Z = 457 mm

Figure 6-1. Power Output versus Heat Input for ESOR-IIA (650°C, Z = 457 mm)

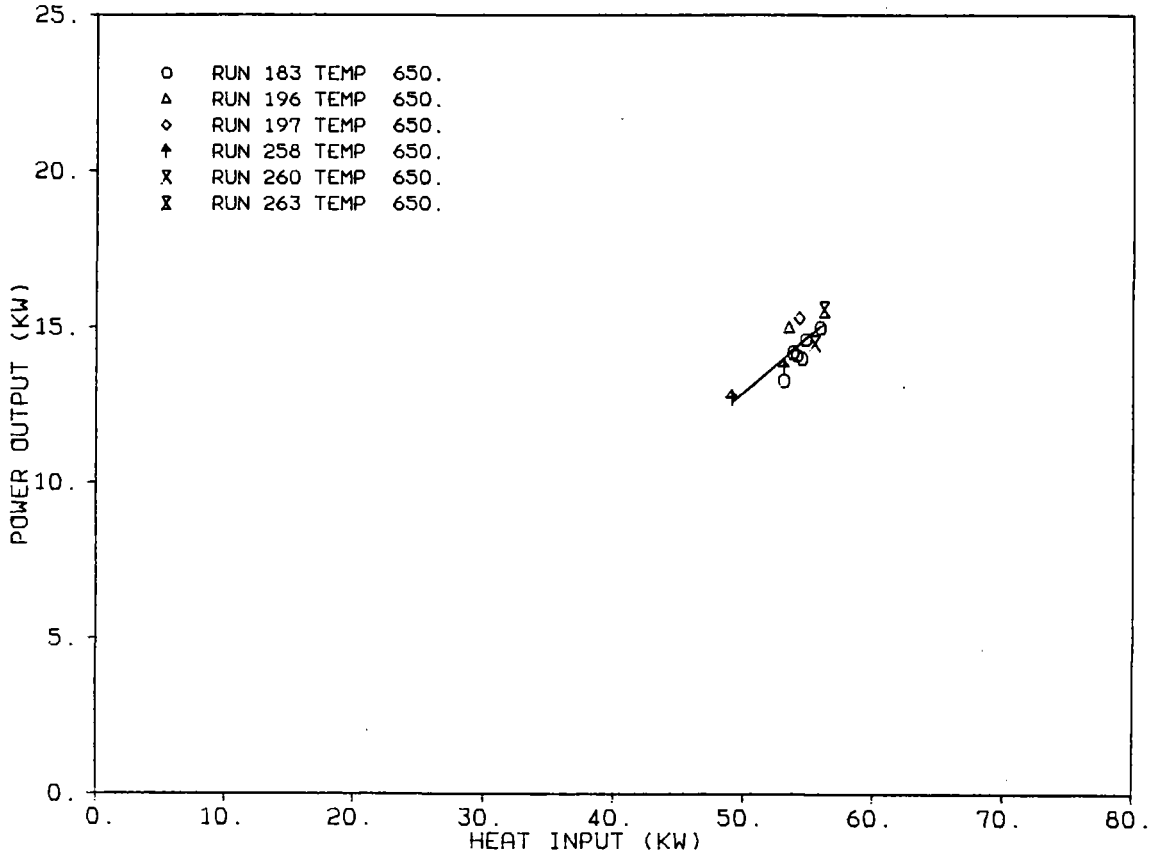

NDEG,SIGFAC 1 .5256

P = .00000000 1.00000000 -5.07575673 .35962198

RUN	X	Y	YFIT	R
183	53.100	13.3	14.020	-.720
183	53.800	14.2	14.272	.072
183	54.100	14.1	14.380	-.280
183	54.500	14.0	14.524	-.524
183	54.800	14.6	14.632	-.032
183	55.900	15.0	15.027	-.027
196	53.500	15.0	14.164	.836
197	54.000	15.3	14.452	.848
258	53.100	13.8	14.020	-.250
258	49.100	12.7	12.582	.158
260	55.500	14.5	14.883	-.403
263	56.200	15.6	15.135	.465

TBC-2
ESOR-IIA, He, full radiator, no window
T = 650°C
Z = 482 mm

Figure 6-2. Power Output versus Heat Input for ESOR-IIA (650°C, Z = 482 mm)

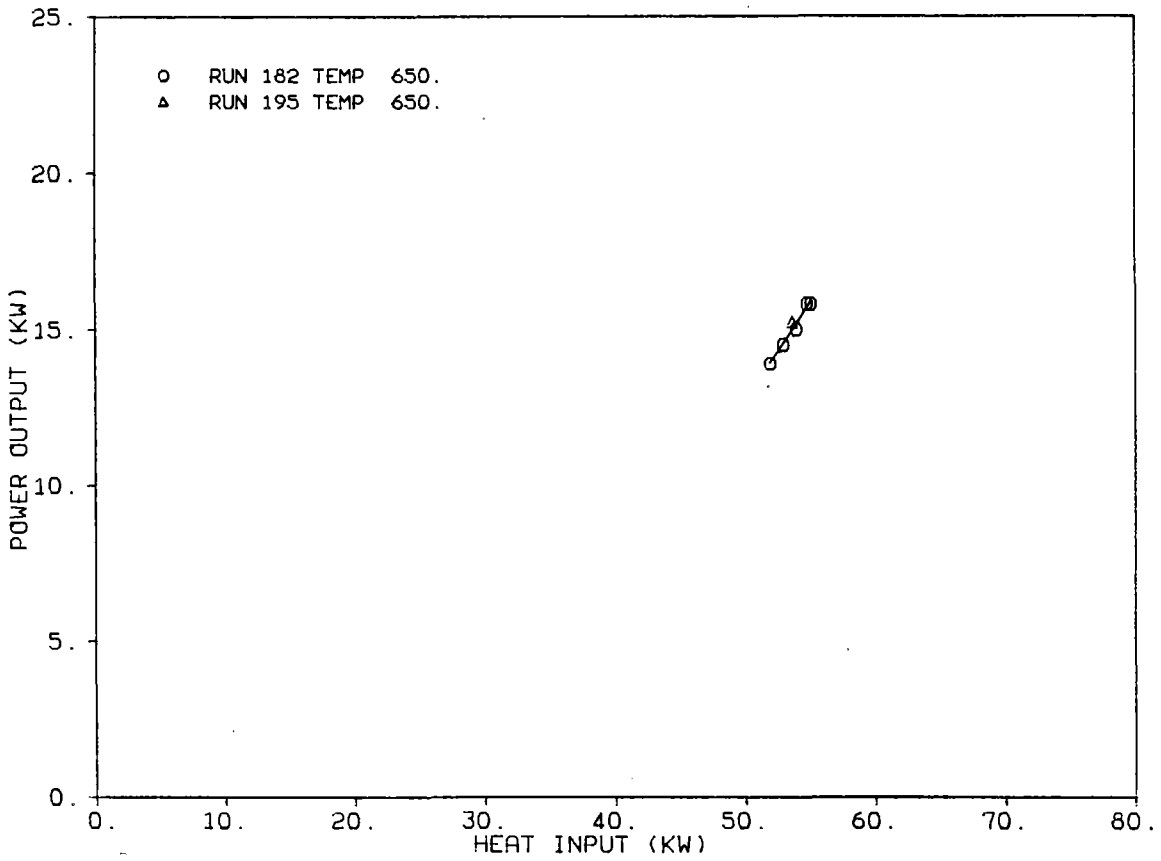

NDEG,SIGFAC 1 .1561

P = .00000000 1.00000000 -19.10342813 .63608874

RUN	X	Y	YFIT	R	
182	51.900	13.9	13.910	-.010	TBC-2
182	52.900	14.5	14.546	-.046	ESOR-IIA, He, full
182	53.900	15.0	15.182	-.182	radiator, no window
182	54.700	15.8	15.691	.109	T = 650°C
182	55.000	15.8	15.881	-.081	Z = 507 mm
195	53.600	15.2	14.991	.209	

Figure 6-3. Power Output versus Heat Input for ESOR-IIA (650°C, Z = 507 mm)

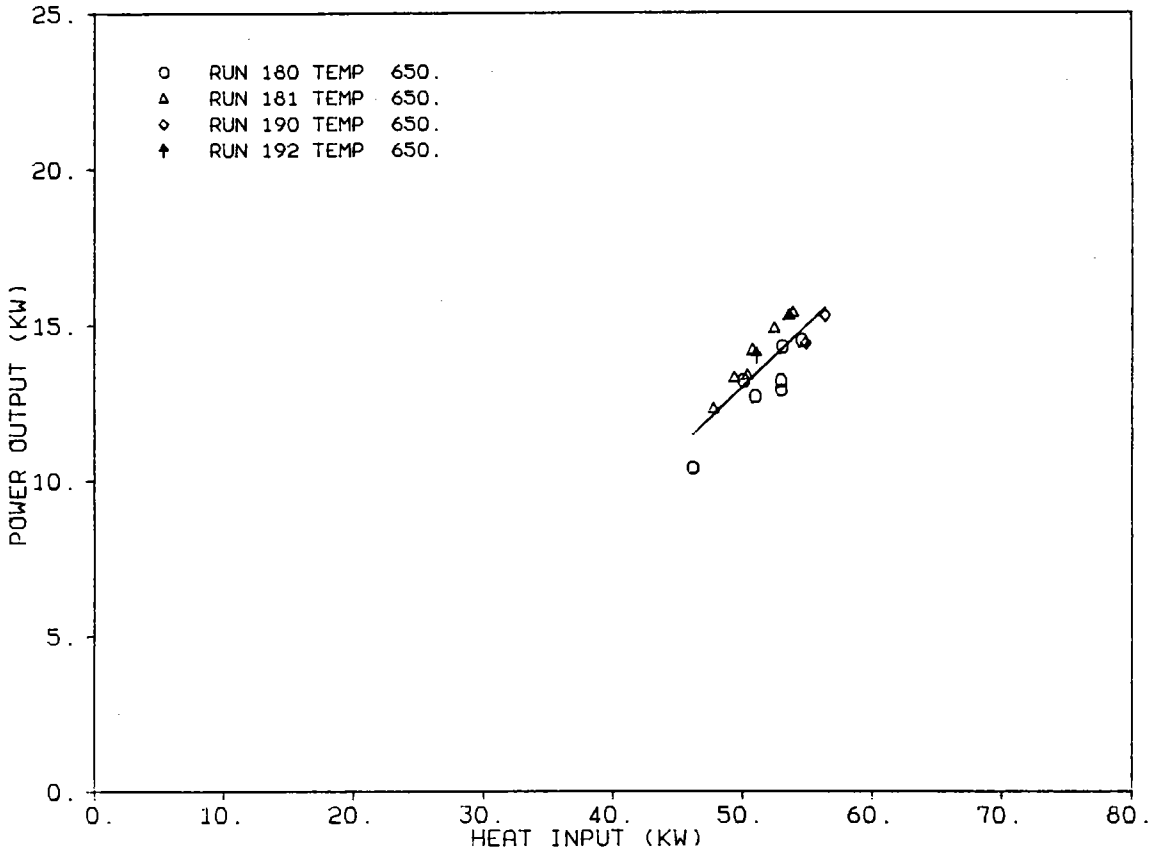

NDEG,SIGFAC 1 .7571

P = .00000000 1.00000000 -7.04283255 .40080307

RUN	X	Y	YFIT	R
180	46.200	10.4	11.474	-1.074
180	51.000	12.7	13.398	-.698
180	53.000	13.2	14.200	-1.000
180	53.100	14.3	14.240	.060
180	54.600	14.5	14.841	-.341
180	50.100	13.2	13.037	.163
180	53.000	12.9	14.200	-1.300
181	47.800	12.3	12.116	.184
181	50.400	13.4	13.158	.242
181	52.500	14.9	13.999	.901
181	53.900	15.4	14.560	.840
181	49.400	13.3	12.757	.543
181	50.800	14.2	13.318	.882
181	53.600	15.3	14.440	.860
190	54.900	14.4	14.961	-.561
190	56.400	15.3	15.562	-.262
192	51.100	14.0	13.438	.562

TBC-2
ESOR-IIA, He, full radiator, no window
T = 650°C
Z = 532 mm

Figure 6-4. Power Output versus Heat Input for ESOR-IIA (650°C, Z = 532 mm)

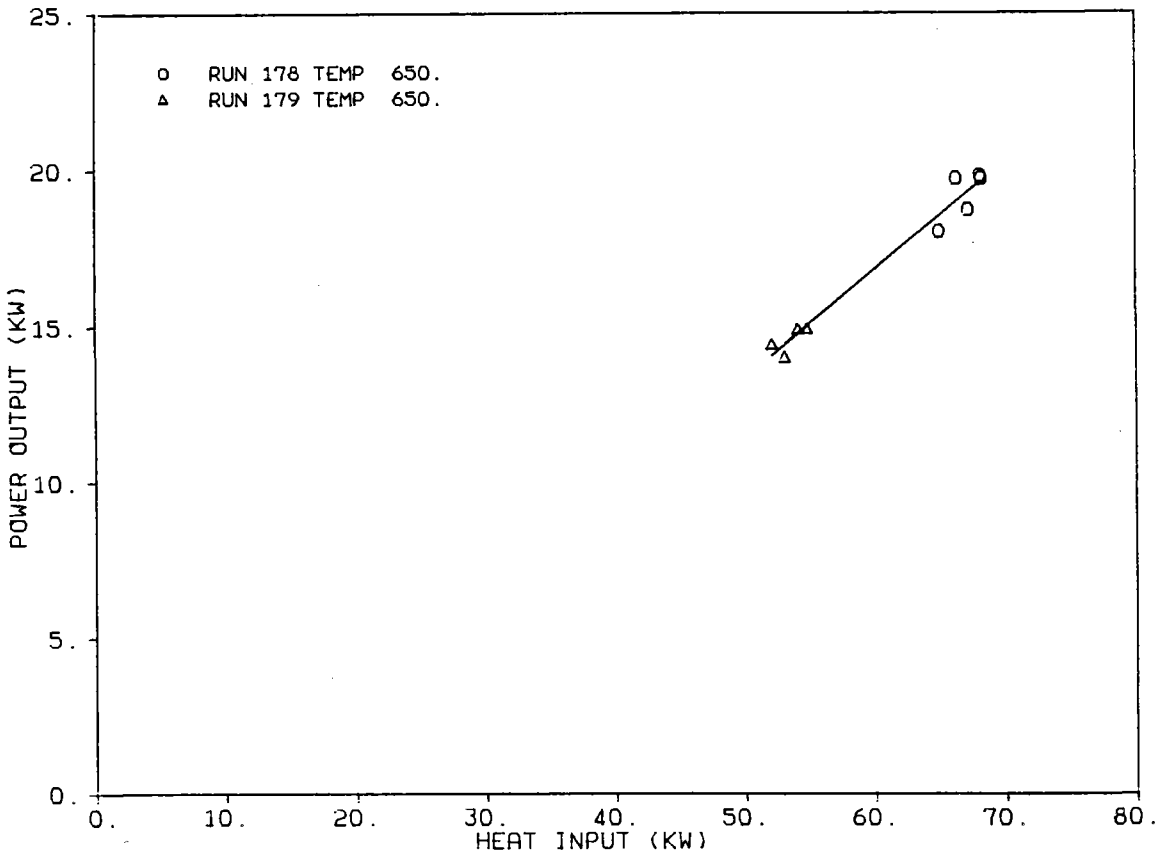

NDEG,SIGFAC 1 .4629

P = .00000000 1.00000000 -3.95404226 .34557548

RUN	X	Y	YFIT	R
178	67.200	18.7	19.269	-.569
178	68.200	19.7	19.614	.086
178	68.100	19.8	19.580	.220
178	66.300	19.7	18.958	.742
178	65.00	18.0	18.508	-.508
179	53.100	14.0	14.396	-.396
179	54.100	14.9	14.742	.158
179	54.800	14.9	14.983	-.083
179	52.100	14.4	14.050	.350

TBC-2
ESOR-IIA, He, full radiator, no window
T = 650°C
Z = 557 mm

Figure 6-5. Power Output versus Heat Input for ESOR-IIA (650°C, Z = 557 mm)

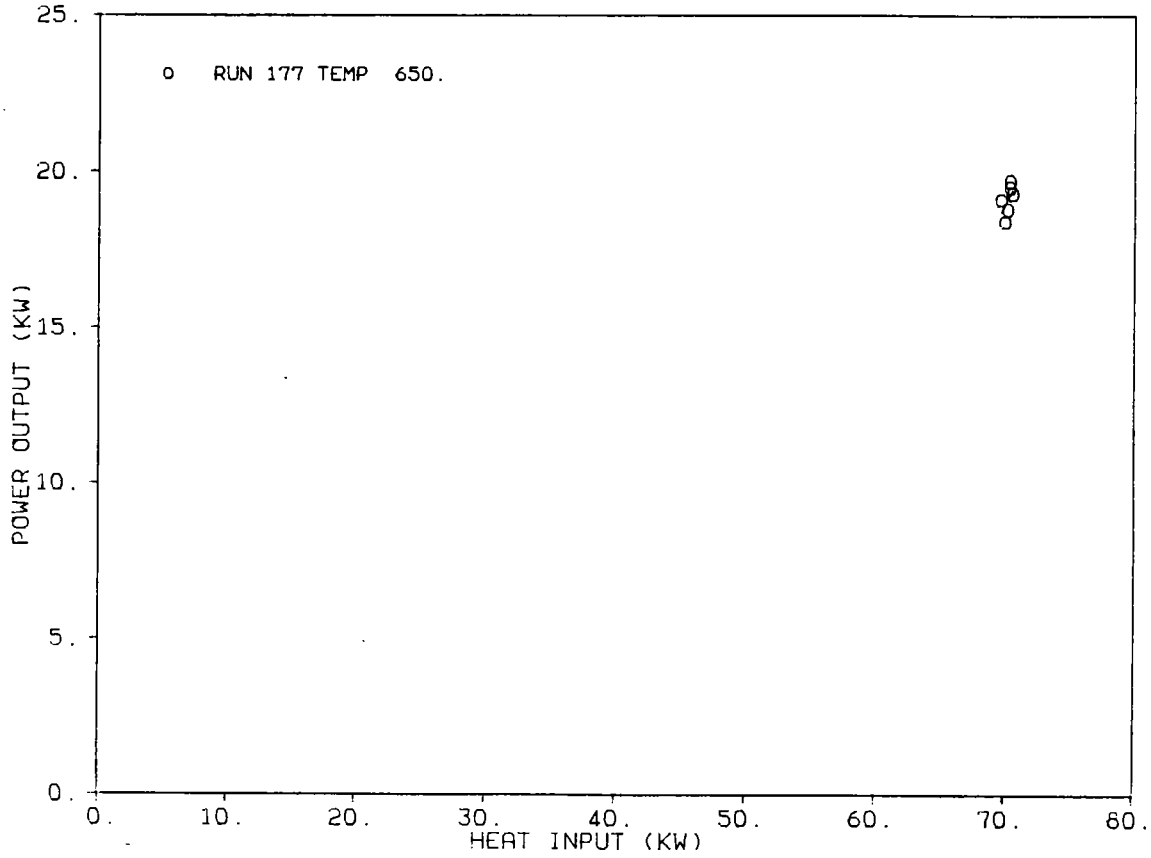

NDEG,SIGFAC 1 .4485

P = .00000000 1.00000000 -36.24253368 .78864279

RUN	X	Y	YFIT	R
177	70.000	18.4	18.962	-.562
177	70.400	19.5	19.278	.222
177	70.600	19.3	19.436	-.136
177	70.400	19.7	19.278	.422
177	70.200	18.8	19.120	-.320
177	69.700	19.1	18.726	.374

TBC-2
ESOR-IIA, He, full radiator, no window
T = 650°C
Z = 582 mm

Figure 6-6. Power Output versus Heat Input for ESOR-IIA (650°C, Z = 582 mm)

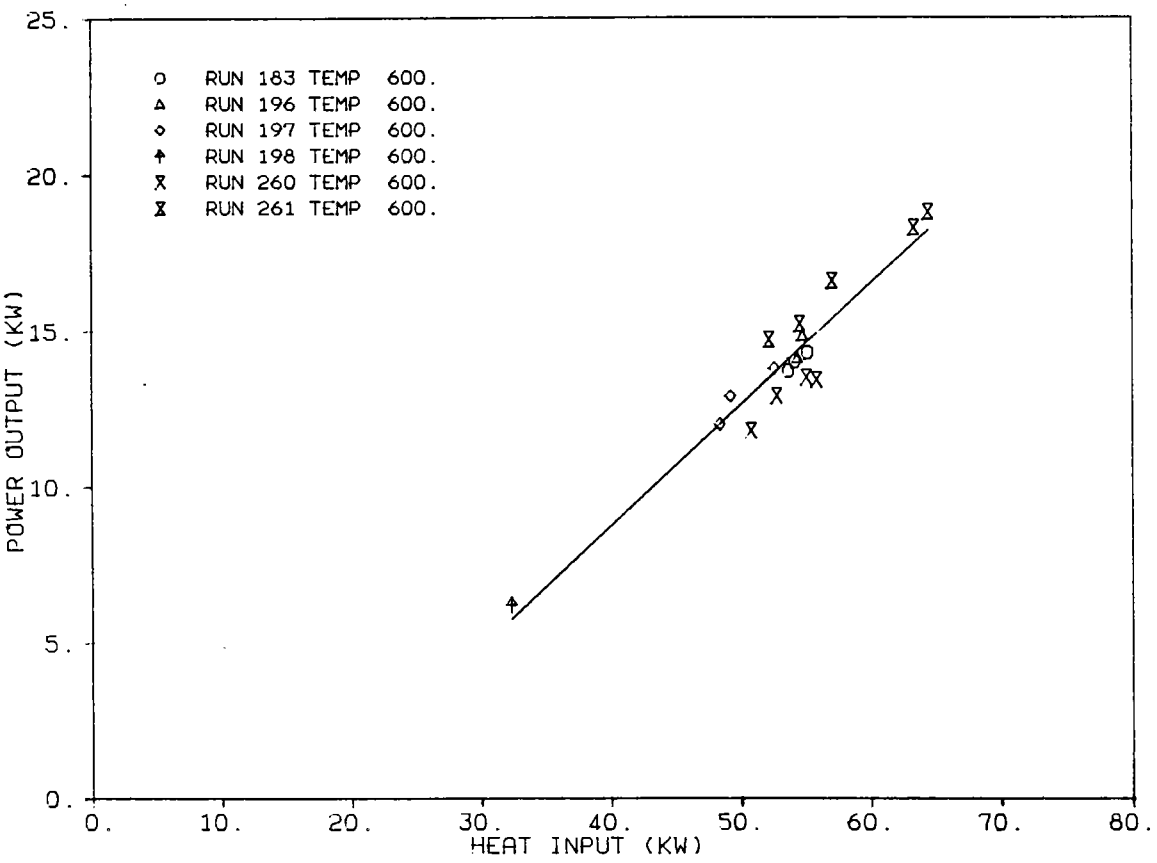

NDEG,SIGFAC 1 .8179

P = .00000000 1.00000000 -6.82066178 .38894060

RUN	X	Y	YFIT	R
183	53.700	13.7	14.065	-.365
183	54.200	14.0	14.260	-.260
183	55.200	14.3	14.649	-.349
196	54.400	14.1	14.338	-.238
196	54.800	14.8	14.493	.307
197	48.400	12.0	12.004	-.004
197	49.200	12.9	12.315	.585
197	52.600	13.8	13.638	.162
198	32.300	6.2	5.742	.458
260	50.800	11.8	12.938	-1.138
260	52.800	12.9	13.715	-.815
260	55.100	13.5	14.610	1.110
260	55.900	13.4	14.921	-1.521
261	52.200	14.7	13.482	1.218
261	54.600	15.2	14.415	.785
261	57.100	16.6	15.388	1.212
261	63.300	18.3	17.799	.501
261	64.400	18.8	18.227	.573

TBC-2
ESOR-IIA, He, full radiator, no window
T = 600°C
Z = 482 mm

Figure 6-7. Power Output versus Heat Input for ESOR-IIA (600°C, Z = 482 mm)

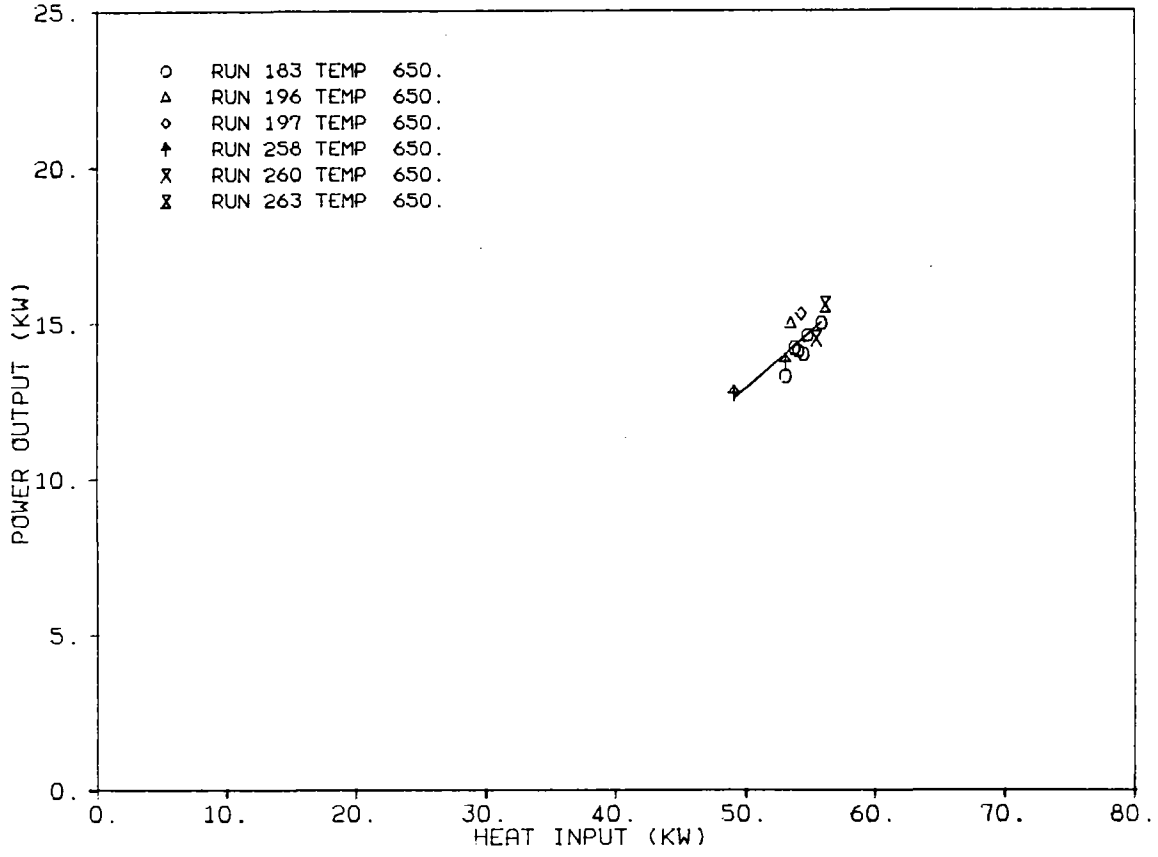

NDEG,SIGFAC 1 .5256

P = .00000000 1.00000000 -5.07575673 .35962198

RUN	X	Y	YFIT	R
183	53.100	13.3	14.020	-.720
183	53.800	14.2	14.272	-.072
183	54.100	14.1	14.380	-.280
183	54.500	14.0	14.524	-.524
183	54.800	14.6	14.632	-.032
183	55.900	15.0	15.027	-.027
196	53.500	15.0	14.164	.836
197	54.300	15.3	14.452	.848
258	53.100	13.8	14.020	-.250
258	49.100	12.7	12.582	.158
260	55.500	14.5	14.883	-.403
263	56.200	15.6	15.135	.465

TBC-2
ESOR-IIA, He, full
radiator, no window
T = 650°C
Z = 482 mm

Figure 6-8. Power Output versus Heat Input for ESOR-IIA (650°C, Z = 482 mm)

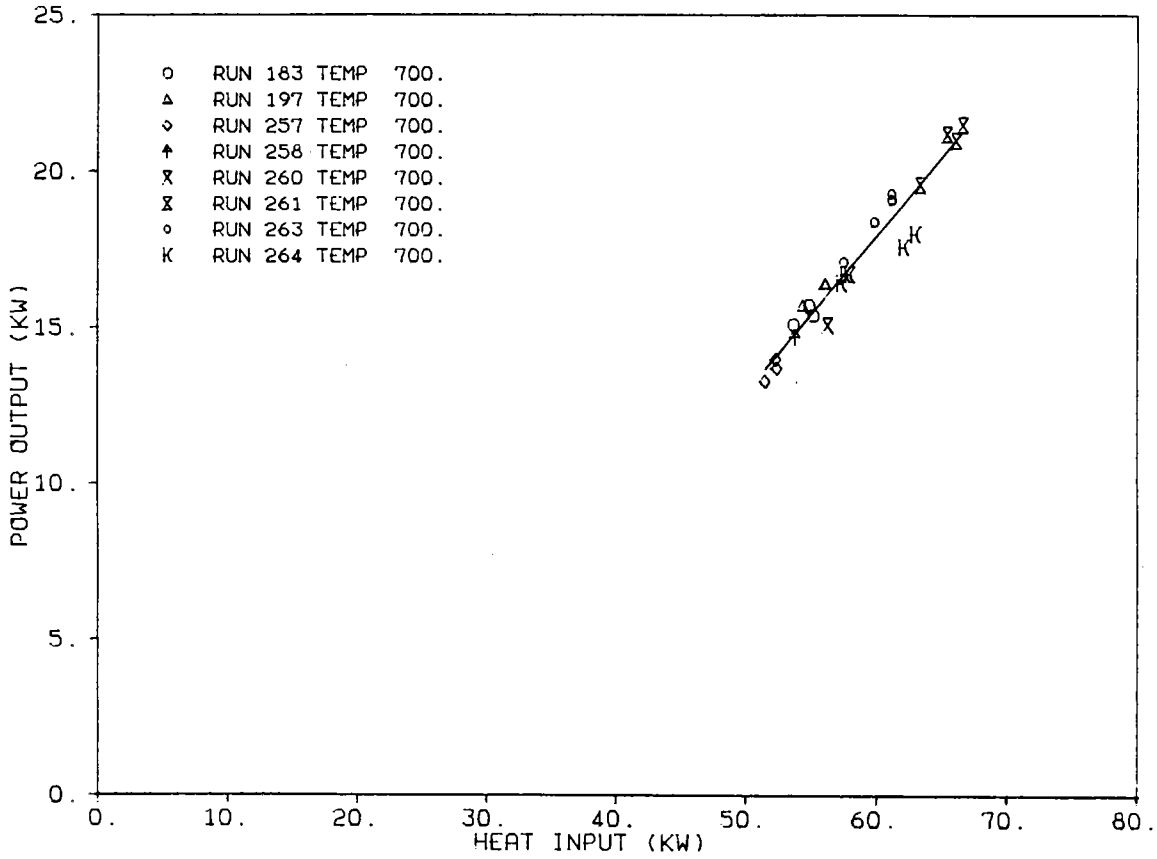

NDEG,SIGFAC 1 .5992

P = .00000000 1.00000000 -12.31771851 .50435407

RUN	X	Y	YFIT	R
183	55.200	15.4	15.523	-.123
183	54.900	15.7	15.371	.329
183	53.700	15.1	14.766	.334
197	56.100	16.4	15.977	.423
197	56.100	16.4	15.977	.423
197	54.400	15.7	15.119	.581
257	51.500	13.3	13.657	-.357
257	52.400	13.7	14.110	-.410
257	52.300	14.0	14.060	-.060
258	53.800	14.7	14.817	-.117
260	56.300	15.1	16.077	-.977
261	65.400	21.2	20.667	.533
261	66.100	21.0	21.020	-.020
261	66.600	21.5	21.272	.228
261	63.300	19.6	19.608	-.008
263	57.500	17.1	16.683	.417
263	59.800	18.4	17.843	.557
263	61.100	19.1	18.498	.602
263	61.100	19.3	18.498	.802
264	57.300	16.4	16.582	-.182
264	57.600	16.7	16.733	-.033
264	57.900	16.7	16.884	-.184
264	62.000	17.6	18.952	-1.352
264	62.900	18.0	19.406	-1.406

TBC-2
ESOR-IIA, He, full radiator, no window
T = 700°C
Z = 482 mm

Figure 6-9. Power Output versus Heat Input for ESOR-IIA (700°C, Z = 482 mm)

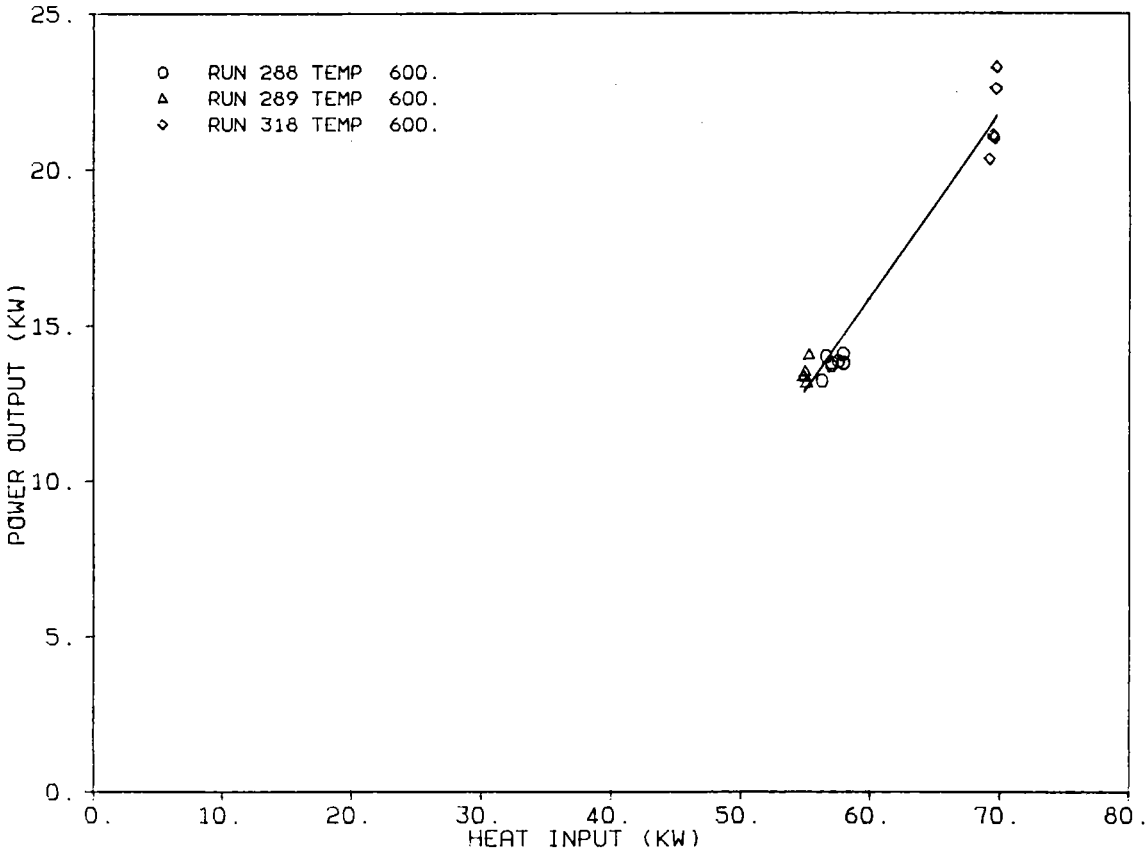

NDEG,SIGFAC 1 .7573

P = .00000000 1.00000000 -19.69388509 .59304360

RUN	X	Y	YFIT	R
288	57.970	13.8	14.685	-.895
288	57.970	14.1	14.685	-.605
288	57.540	13.8	14.430	-.600
288	57.050	13.8	14.139	-.339
288	56.980	13.7	14.098	-.388
288	56.630	14.0	13.890	.110
288	56.280	13.2	13.683	-.463
289	54.870	13.4	12.846	.514
289	55.010	13.5	12.929	.591
289	55.150	13.2	13.012	.158
289	54.940	13.4	12.888	.492
289	55.300	14.1	13.101	.969
318	69.480	21.1	21.511	-.421
318	69.560	21.0	21.558	-.548
318	69.210	20.3	21.351	-1.031
318	69.830	23.3	21.718	-1.552
318	69.740	22.6	21.665	.905

TBC-1
ESOR-IIA, He, full
radiator, no window
T = 600°C
Run 318 was conducted
after rod replacement

Figure 6-10. Power Output versus Heat Input for ESOR-IIA (600°C)

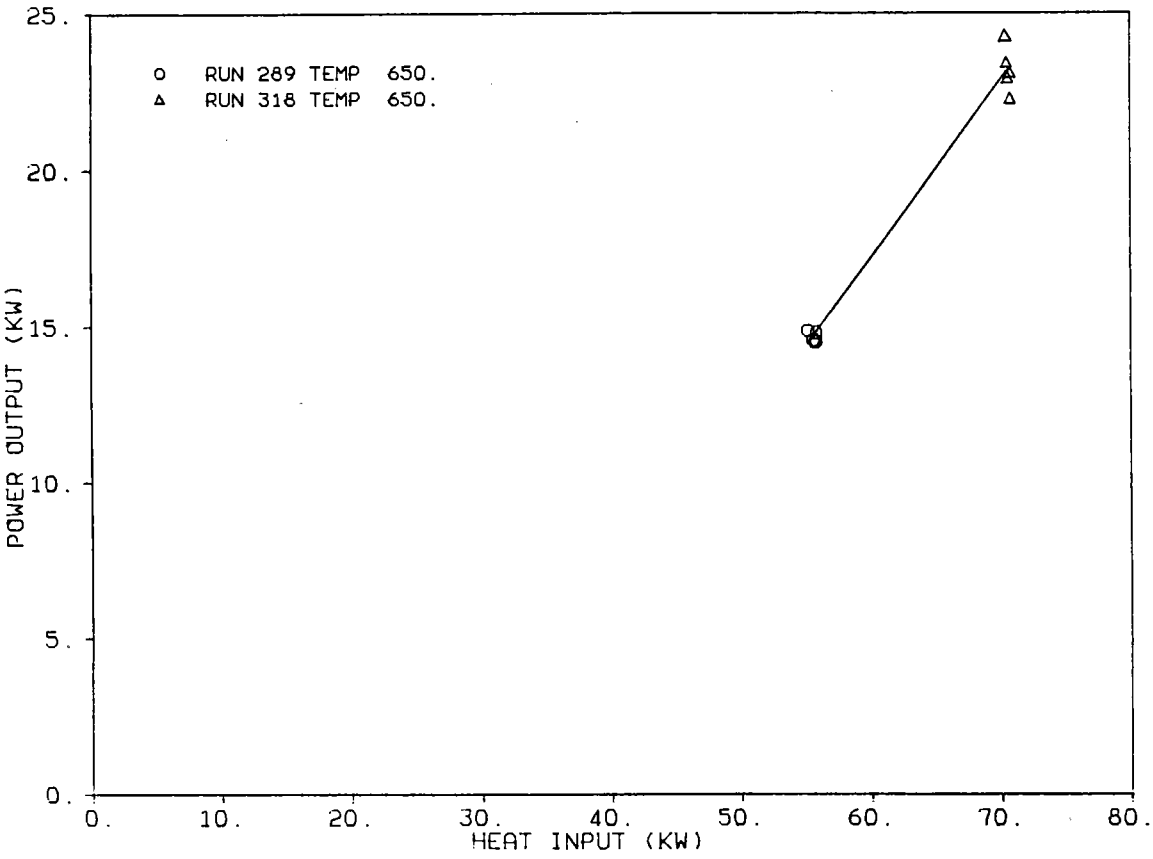

NDEG,SIGFAC 1 .6067

P = .00000000 1.00000000 -17.06912208 .56962340

RUN	X	Y	YFIT	R
289	55.930	14.8	14.790	-.010
289	55.860	14.5	14.750	-.240
289	55.650	14.5	14.630	-.090
289	55.790	14.5	14.710	-.170
289	55.240	14.9	14.397	.463
318	70.530	23.4	23.106	.294
318	70.440	24.2	23.055	1.195
318	70.790	23.1	23.255	-.185
318	70.790	22.2	23.255	-1.015
318	70.610	22.9	23.152	-.242

TBC-1
ESOR-IIA, He, full radiator, no window
T = 650°C

Figure 6-11. Power Output versus Heat Input for ESOR-IIA (650°C)

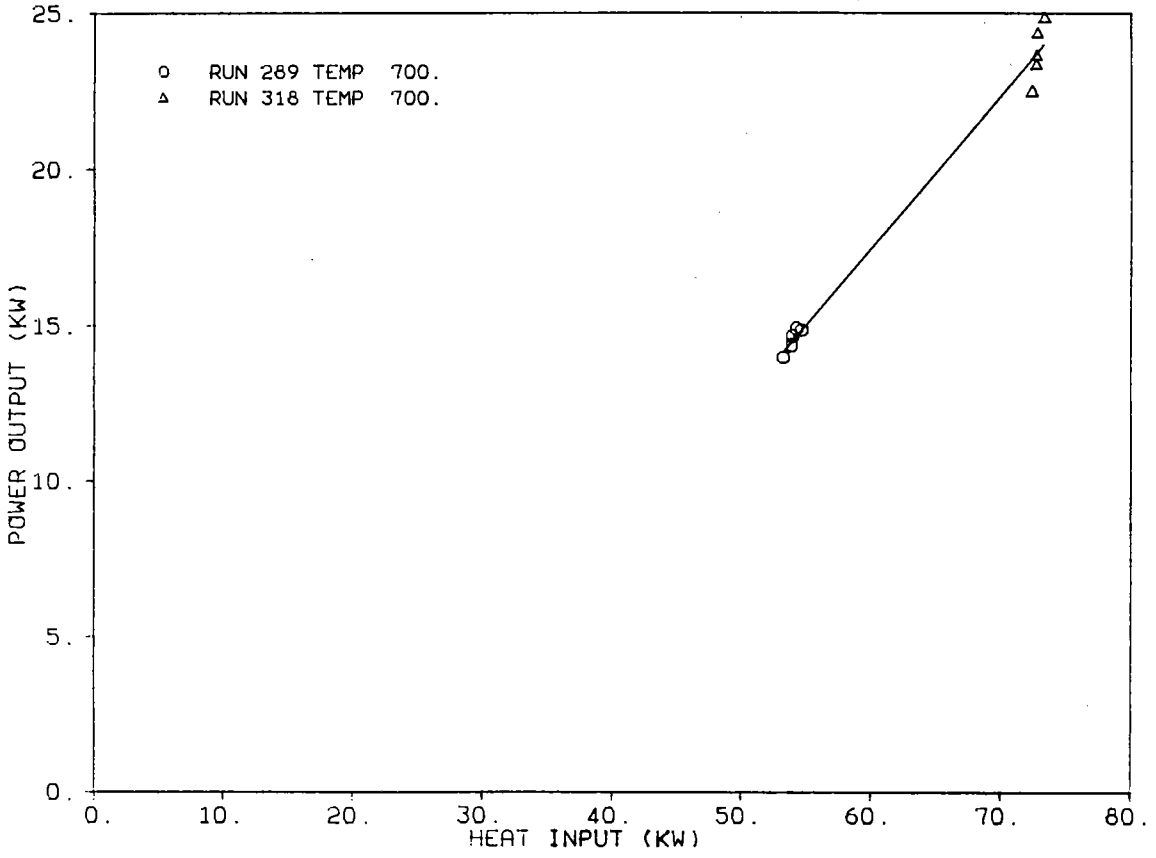

NDEG,SIGFAC 1 .5491

P = .00000000 1.00000000 -11.90176165 .48971200

RUN	X	Y	YFIT	R
289	54.660	14.9	14.866	-.006
289	53.960	14.7	14.523	.137
289	54.240	14.9	14.660	.250
289	53.890	14.4	14.489	-.119
289	53.260	14.0	14.180	-.200
318	72.360	22.5	23.534	-1.044
318	72.730	23.3	23.715	-.375
318	72.730	23.7	23.715	-.065
318	73.340	24.8	24.014	.836
318	72.810	24.3	23.754	.586

TBC-1
ESOR-IIA, He, full
radiator, no window
T = 700°C

Figure 6-12. Power Output versus Heat Input for ESOR-IIA (700°C)

C. ESOR-IIB WITH HELIUM, FULL RADIATOR, AND NO WINDOW (CATEGORY NO. 2)

Figure 6-13 and its accompanying table present the performance of the TBC-2/ESOR-IIB/USAB 4-95 (helium) configuration at 700°C. A heater tube-cylinder head axial position of Z = 482 mm existed during these tests. These data result in reasonable values for both the Q_{in}-axis intercept and dP_{out}/dQ_{in}. However, this must be considered largely fortuitous because the tests were performed at virtually full load and thus produced imprecise data. Comparison of these results with those presented by Figure 6-9 and its accompanying table shows that, to the accuracy of the data, an extension of the linear least squares best fit (LSBF) of the data for either receiver represents the other data set reasonably well. Thus, it must be concluded on the basis of this comparison that, so far as power conversion assembly (PCA) performance is concerned, there is no reason to prefer ESOR-IIB to ESOR-IIA or vice versa.

Within the range of the experimental data, i.e., $40 < Q_{in} < 50$, comparison of Figure 6-13 and its accompanying table to Figure 6-1 and the associated linear LSBF of the corresponding data as presented in Appendix B-IV leads to the following:

TBC-2/ESOR-IIB/USAB 4-95 (H_2): $P_{out} = -8.395 + .4732\ Q_{in}$

and

TBC-1/ESOR-IIB/USAB 4-95 (He): $P_{out} = -8.081 + .411\ Q_{in}$

Thus, at Q_{in} = 45 kWt, $P_{out_{H_2}} - P_{out_{He}} = 12.90 - 10.42 = 2.48$ kWe

and, at Q_{in} = 60 kWt, $P_{out_{H_2}} - P_{out_{He}} = 20.00 - 16.59 = 3.41$ kWe.

The reader is cautioned once more that the range of Q_{in} represented in Figure 6-13 is insufficient to establish dP_{out}/dQ_{in} to the accuracy required for the extrapolation of the corresponding linear LSBF curve to 60 kWt. It seems more likely to the author that $P_{out_{H_2}} - P_{out_{He}}$ remains at about 2.5 kWe from 30 kWt $\leq Q_{in} \leq$ 70 kWt in the cases under consideration here. Further comparisons of other configurations, identical except for the working gas employed, will be made in later paragraphs of this discussion.

D. ESOR-IIA WITH HELIUM, FULL RADIATOR, AND WINDOW (CATEGORY NO. 3)

One extensive series of tests incorporated a quartz window into the receiver of the TBC-2/ESOR-IIA/USAB 4-95 (helium) configuration. The windows employed were placed within the receiver's cavity rather than directly across its aperture. The performances of the configuration relative to the otherwise identical windowless configuration were inferior at both 600 and 700°C heater head average gas temperature, cf. Figures 6-14 and 6-15. At 600°C and at Q_{in} = 60 kWt, the presence of the window decreased P_{out} by about 1.2 kWe; at 700°C and the same Q_{in}, the presence of the window decreased

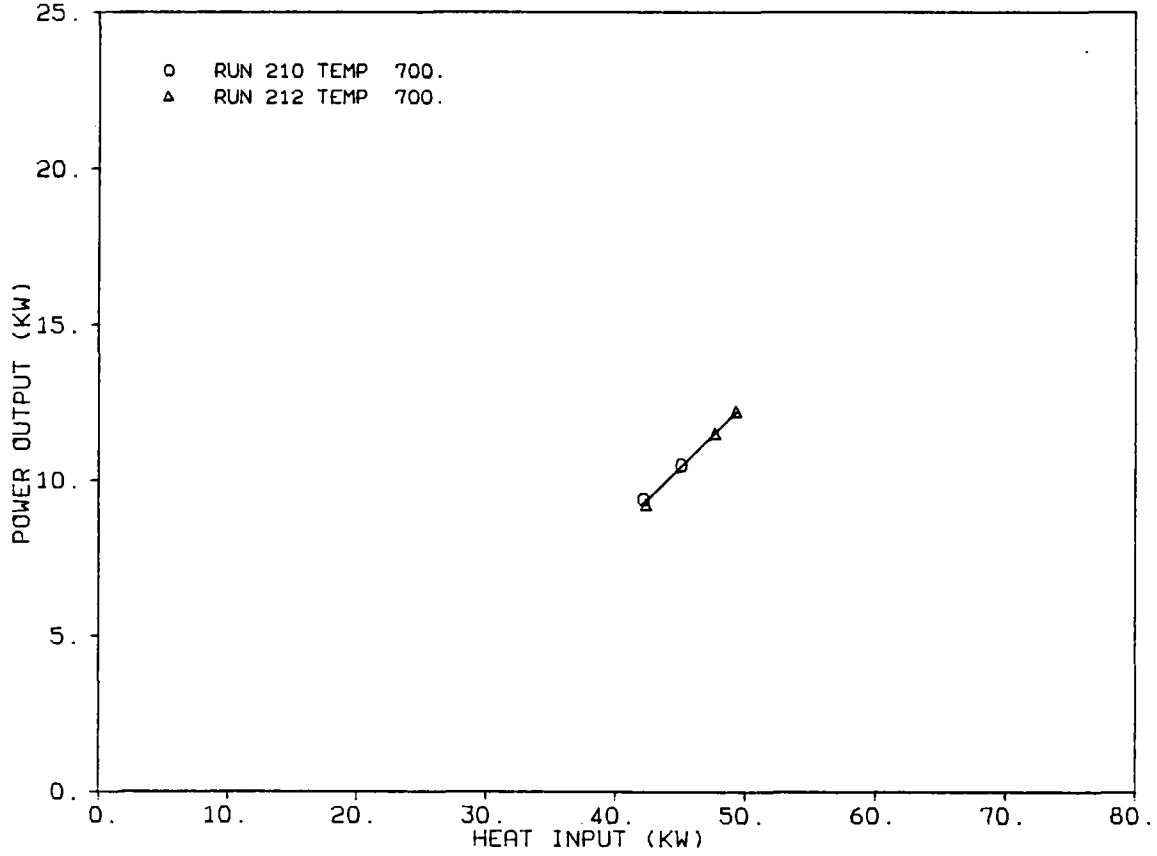

ND EG,SIGFAC 1 .1191

P = .00000000 1.00000000 -8.08074057 .41113234

RUN	X	Y	YFIT	R	
210	42.200	9.4	9.269	.131	TBC-2
210	45.100	10.5	10.461	.039	ESOR-IIB, He, full
212	42.400	9.2	9.351	-.151	radiator, no window
212	47.700	11.5	11.530	-.030	T = 700°C
212	49.300	12.2	12.188	.012	

Figure 6-13. Power Output versus Heat Input for ESOR-IIB (700°C)

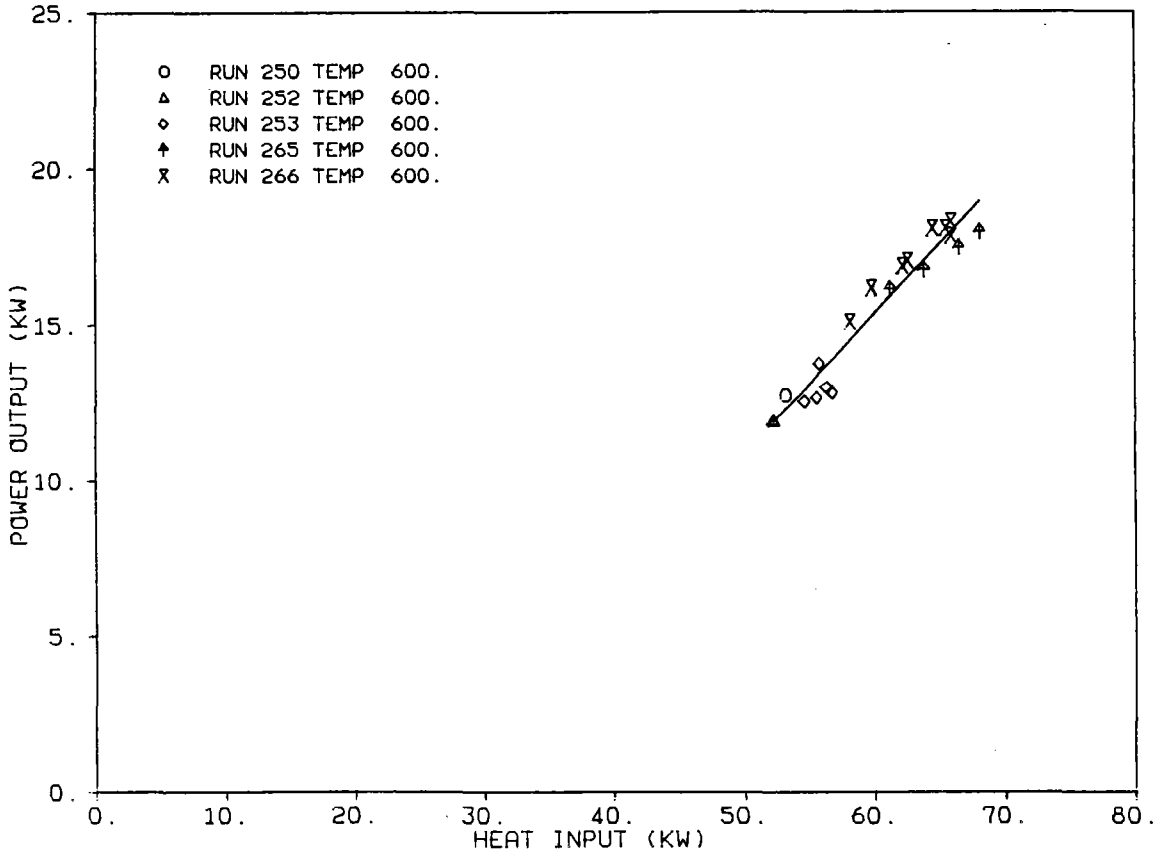

ND EG,SIGFAC 1 .6126

P = .00000000 1.00000000 -11.31237209 .44431829

RUN	X	Y	YFIT	R
250	53.090	12.7	12.276	.464
252	52.170	11.9	11.868	.062
252	52.240	11.9	11.899	-.019
253	54.560	12.5	12.930	-.390
253	55.500	12.7	13.347	-.687
253	55.730	13.7	13.449	.301
253	56.270	13.0	13.689	-.709
253	56.660	12.8	13.863	-1.033
265	61.240	16.1	15.898	.242
265	63.850	16.7	17.057	-.317
265	66.500	17.5	18.235	-.765
265	68.110	18.0	18.950	-.990
266	58.080	15.1	14.494	.596
266	59.790	16.2	15.253	.907
266	62.210	16.9	16.329	.561
266	62.590	17.1	16.498	.562
266	64.530	18.1	17.359	.711
266	65.500	18.1	17.790	.310
266	65.890	17.8	17.964	-.124
266	65.930	18.3	17.982	.318

TBC-2
ESOR-IIA, He, full
radiator, no window
T = 600°C

Figure 6-14. Power Output versus Heat Input for ESOR-IIA (600°C)

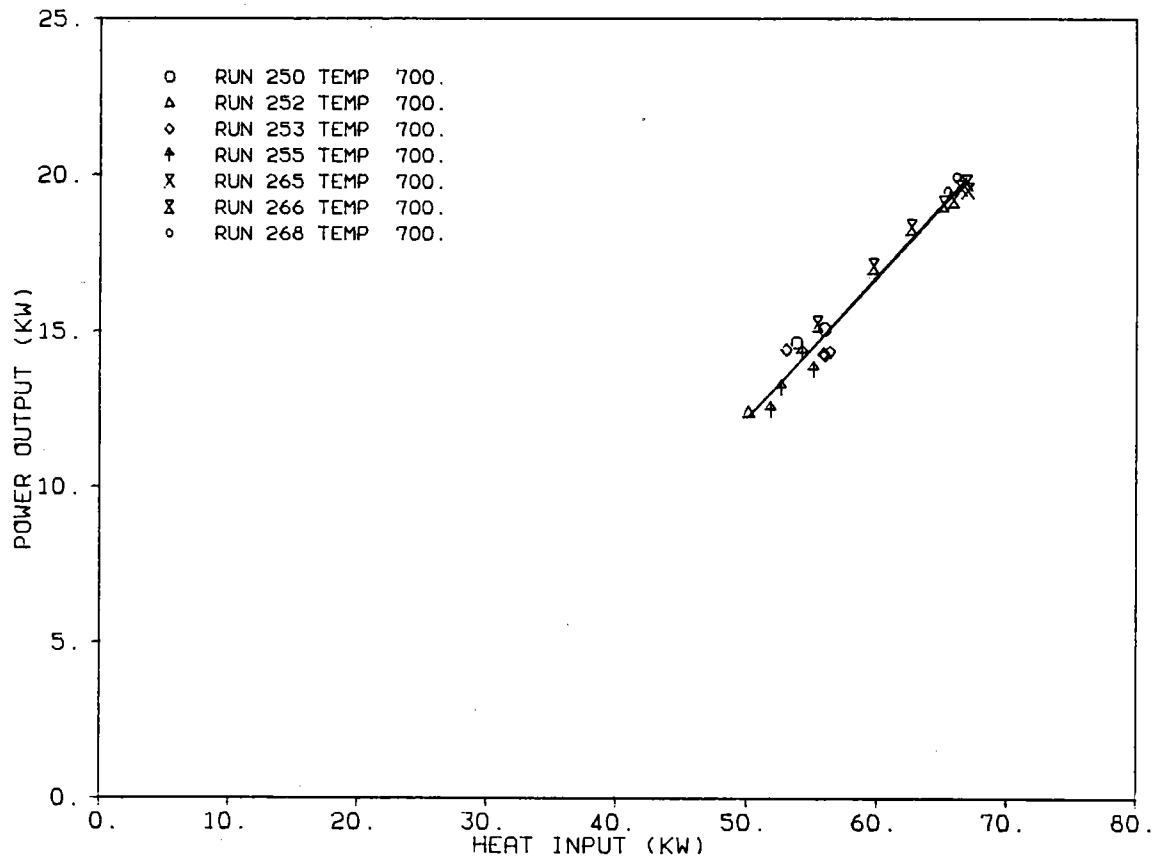

ND EG,SIGFAC 1 .4979

P = .00000000 1.00000000 -10.54319286 .45478958

RUN	X	Y	YFIT	R
250	53.790	14.6	13.920	.730
250	55.960	15.1	14.907	.173
252	50.150	12.4	12.265	.155
253	53.030	14.4	13.574	.836
253	55.880	14.3	14.870	-.580
253	55.960	14.2	14.907	-.667
253	56.420	14.4	15.116	-.756
255	51.780	12.5	13.006	-.516
255	52.630	13.2	13.392	-.172
255	54.250	14.3	14.129	.201
255	55.100	13.8	14.516	-.726
265	66.460	19.6	19.682	-.092
265	66.850	19.7	19.859	-.109
265	66.950	19.5	19.905	-.415
266	55.430	15.2	14.666	.564
266	59.680	17.1	16.599	.481
266	62.590	18.3	17.922	.408
266	65.120	19.1	19.073	.017
266	65.890	19.2	19.423	-.223
268	65.400	19.5	19.200	.270

ESOR-IIA, He, full radiator, with window T = 700°C

Figure 6-15. Power Output versus Heat Input for ESOR-IIA (700°C)

P_{out} by approximately 1.3 kWe. This degradation of receiver performance was predicted by the author of this report. However, funds were not available to perform experimental tests on a thermophysically similar but simpler receiver designed to provide answers to this and other questions regarding receiver operation.

Comparison of Figures 6-14 and 6-15 to determine the performance improvement realized by increasing the heater head average gas temperature of this configuration from 600 to 700°C shows that, over the range 53 kWt < Q_{in} < 66 kWt, P_{out} 700°C - P_{out} 600°C ≈ 1.25 kWe.

E. ESOR-IIA WITH HELIUM, VARIABLE RADIATOR, AND NO WINDOW (CATEGORY NO. 4)

In an investigation of the USAB 4-95 engine cooling system, a series of tests conducted rather late in the parabolic dish Stirling program provided the data presented in Figure 6-16 and the accompanying table. These tests were conducted with the TBC-1/ESOR-IIA/USAB 4-95 (helium) configuration. The axial heater position was Z = 482 mm. A stated purpose of these tests was to reduce the parasitic power required by the cooling system from 3.5 to 4 kWe to less than 1 kWe.

These tests were virtually always conducted when two modules were operated in parallel, and the electric power consumed by the radiator cooling fans was not measured separately for each module nor was it measured separately from other parasitic electrical power consumers such as the cooling water pumps on the modules. Therefore, it is impossible to determine what, if any, effect partial blockage of the radiator air cooling flow may have had on cooling fan power requirements.

Because the cooling fan was a simple axial one and the cooling fan motor was of the ac-induction type, if the fan was operating at anywhere near maximum efficiency in the unblocked condition, the power required to drive the fan when various fractions of the radiator were blocked could change only very little. Therefore, these tests revealed little with respect to reducing radiator cooling fan parasitic power. However, it was possible to determine an approximately optimum radiator area for air flow, given the particular fan and induction motor employed.

During all these tests, the cooling water pump was operated at a volume flow rate of about 113 l/min (30 gal/min), resulting in a cooling water temperature rise of no more than 5°C in the most severe case. A rise in cooling water temperature of 25°C is not uncommon in Otto or Diesel engines of roughly comparable size, and the cooling water requirement for such engines is less than that for the Stirling. In the author's opinion, two possible reasons for such severe restriction on the cooling water temperature rise are concerns regarding:

DEG,SIGFAC 1 .2481

P = .00000000 1.00000000 -7.77243501 .38464593

RUN	X	Y	YFIT	R
324	63.800	16.6	16.768	-.168
324	64.700	16.8	17.114	-.314
324	65.300	17.3	17.345	-.045
324	66.700	17.9	17.883	.017
324	66.700	17.5	17.883	-.383
324	67.600	18.4	18.230	.170
326	60.600	15.6	15.537	.063
326	62.900	16.4	16.422	-.022
326	63.400	16.6	16.614	-.014
326	65.400	17.2	17.383	-.183
326	64.600	17.2	17.076	.124
326	65.000	16.8	17.230	-.430
329	71.500	19.7	19.730	-.030
329	72.600	20.3	20.153	.147
329	72.800	19.7	20.230	-.530
329	72.100	20.1	19.961	.139
329	72.500	20.2	20.114	.086
329	72.500	20.5	20.114	.386
331	69.800	18.8	19.076	-.276
331	70.000	19.1	19.153	-.053
331	69.400	19.1	18.922	.178
331	68.700	19.1	18.653	.447
331	68.200	18.1	18.460	-.360
332	68.200	18.3	18.460	-.160
332	68.600	18.8	18.614	.186
332	67.000	18.3	17.999	.301
332	65.300	17.8	17.345	.455
332	65.100	17.5	17.268	.232
334	66.000	17.4	17.614	-.214
334	67.500	18.3	18.191	.109
334	67.400	18.1	18.153	-.053
334	67.600	18.2	18.230	-.030
334	67.000	18.0	17.999	.001
334	67.500	18.0	18.191	-.191
334	66.800	17.9	17.922	-.022
334	66.700	17.9	17.883	.017
334	66.000	17.8	17.614	.186
334	65.200	17.7	17.306	.394
336	66.500	17.8	17.807	-.007
336	67.500	18.3	18.191	.109
336	68.500	18.0	18.576	-.576
336	68.200	18.1	18.460	-.360
336	67.500	18.3	18.191	.109
336	66.100	17.9	17.653	.247
338	68.200	18.7	18.460	.240
338	68.000	18.4	18.383	.017
338	68.400	18.6	18.537	.063

TBC-1
ESOR-IIA, He, variable
radiator, no window
T = 700°C
Z = 532 mm
Tests with various
fractions of the total
radiator air-side
cross-section covered

All runs completed
after rod replacement.

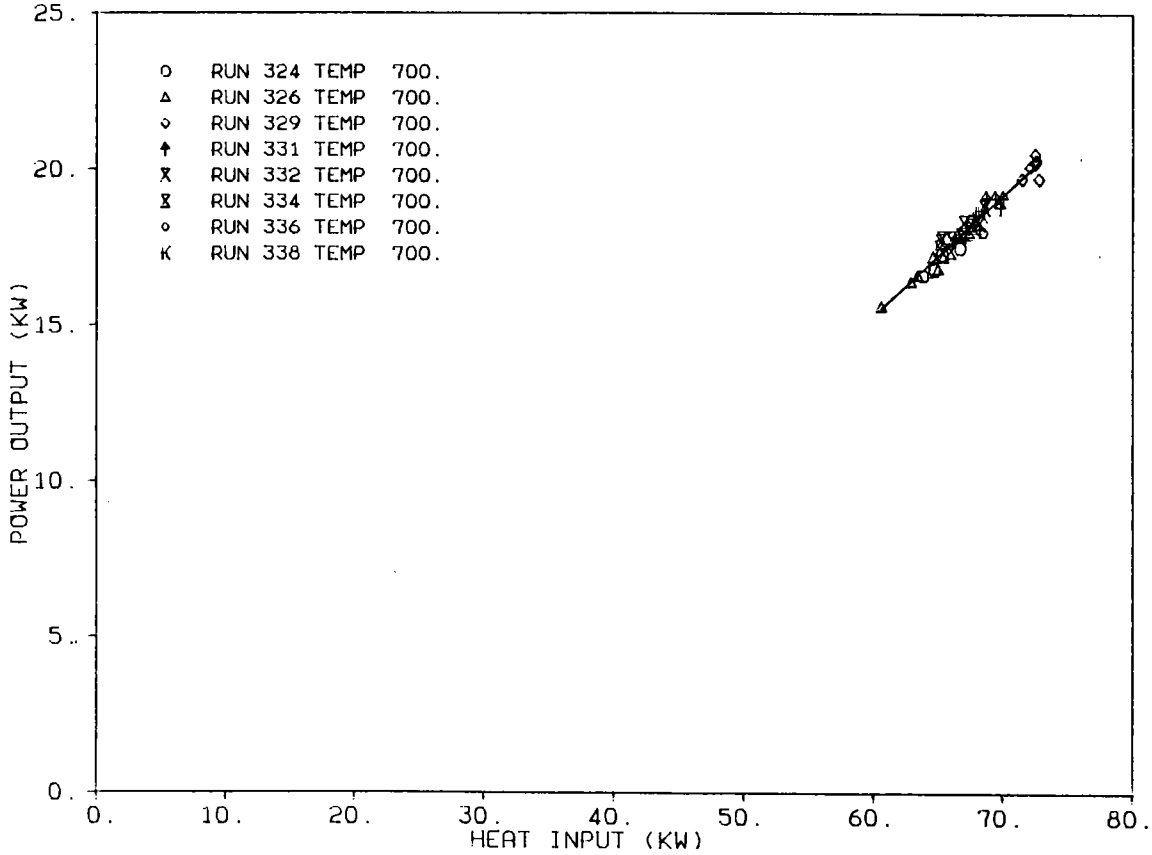

Figure 6-16. Power Output versus Heat Input for ESOR-IIA (700°C, Z = 532 mm)

(1) the existence of hot spots in the engine, or

(2) the trapping at high points within the engine cooling passages of air bubbles formed by dissolution from the water as it is heated within the engine.[1]

In summary, the extensive testing of partially covered radiator air flow passages indicates that the radiator core area could probably be reduced by about one half without serious effect on module performance. However, no conclusions are possible regarding how much air cooling fan and water pump parasitic power might be reduced by proper cooling system optimization. Throughout the course of this test program, electrical parasitics between the module and the grid (as indicated by measurements reported in the data printouts during brief periods when only the radiator test module was operating) remained at a little more than 3 kWe.[2]

Comparison of Figures 6-12 and 6-16 and their respectively corresponding tables again indicate the unreliability of dP_{out}/dQ_{in} as determined over short ranges in the variation of Q_{in}. Direct comparison does show that at least 1.5 to perhaps as much as 2.1 kW of electricity are required to drive the water pump and air fan of the focal-point-mounted cooling system employed in the radiator coverage tests. The reason this difference appears between the two configurations is that, in the tests corresponding to Figure 6-16, the required water pump and cooling fan parasitic requirements of the focal-point-mounted cooling system are extracted above the point in the alternator output circuit where P_{out} is measured, while the parasitic requirements of the ground-mounted radiator, cooling pump, and air fan assembly employed in the tests represented by Figure 6-12 are extracted beyond the point in the alternator output circuit where P_{out} is measured.

F. ESOR-III WITH HYDROGEN (CATEGORY NO. 5) AND ESOR-III WITH HELIUM (CATEGORY NO. 6)

The TBC-2/ESOR-III/USAB 4-95 (hydrogen and helium) test results are presented in Figure 6-17 and Figures 6-18 through 6-20 and their corresponding tables. In contrast to many of the earlier tests, the test data corresponding to Figures 6-17 and 6-18 span appreciable ranges of heat power input; thus, the linear LSBF curves provide reasonable values of dP_{out}/dQ_{in}; unfortunately, the extrapolations to the intercepts with the P_{out} axes are too great to provide more than crude estimates of these intercepts.

---

[1] A private communication with H. Nelving of USAB suggests the following reasons for the high water flow: "(1) to lower the temperature level on the cold side to improve the efficiency and (2) to get a uniform temperature in all Stirling cycles, with the buildup of the engine as USAB has, and also a uniform cooling on all components such as coolers, cylinder liners, O-rings, pistons, connectors, etc., in the cylinder block."

[2] A private communication by H. Nelving of USAB reads: "In my files, I have a measurement of the parasitics, separately measured, without an operating engine. The water pump power consumption is 200 W, low speed fan power consumption is 790 W, and high speed fan power consumption is 1230 W. The measurements are from late August 1983."

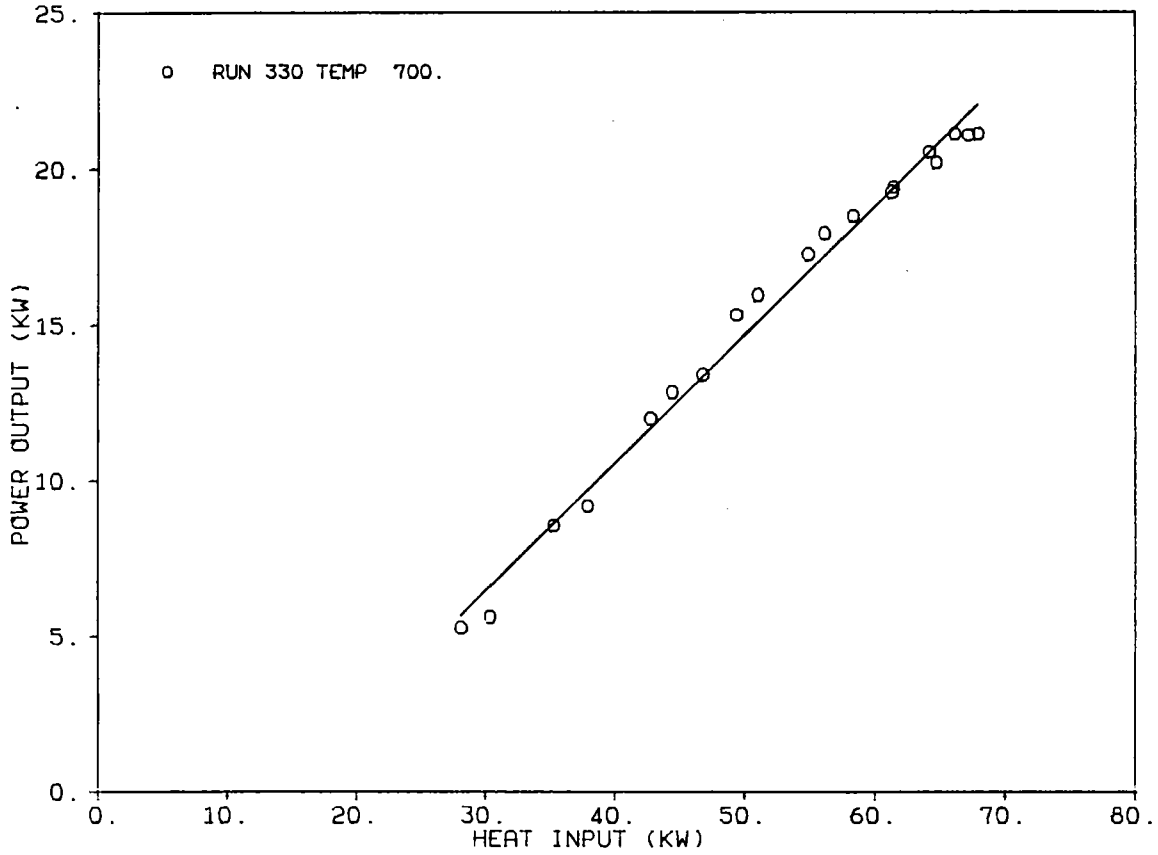

NDEG,SIGFAC 1 .5922

P = .00000000 1.00000000 -5.92135650 .41197540

RUN	X	Y	YFIT	R
330	30.380	5.6	6.594	-.964
330	35.320	8.6	8.630	-.070
330	42.740	12.0	11.686	.314
330	46.740	13.4	13.334	.086
330	50.980	16.0	15.081	.879
330	54.850	17.2	16.675	.575
330	58.300	18.5	18.097	.383
330	61.250	19.2	19.312	-.072
330	64.720	20.2	20.742	-.552
330	67.900	21.1	22.052	-.942
330	67.140	21.1	21.739	-.679
330	66.080	21.1	21.302	-.192
330	64.140	20.5	20.503	.017
330	61.400	19.4	19.374	.016
330	56.110	17.9	17.195	.715
330	49.340	15.3	14.406	.914
330	44.400	12.8	12.370	.470
330	37.900	9.2	9.693	-.503
330	28.150	5.3	5.676	-.396

TBC-2
ESOR-III, H_2, full radiator, no window
T = 700°C
Z = 482 mm

Figure 6-17. Power Output versus Heat Input for ESOR-III with Hydrogen (700°C, Z = 482 mm)

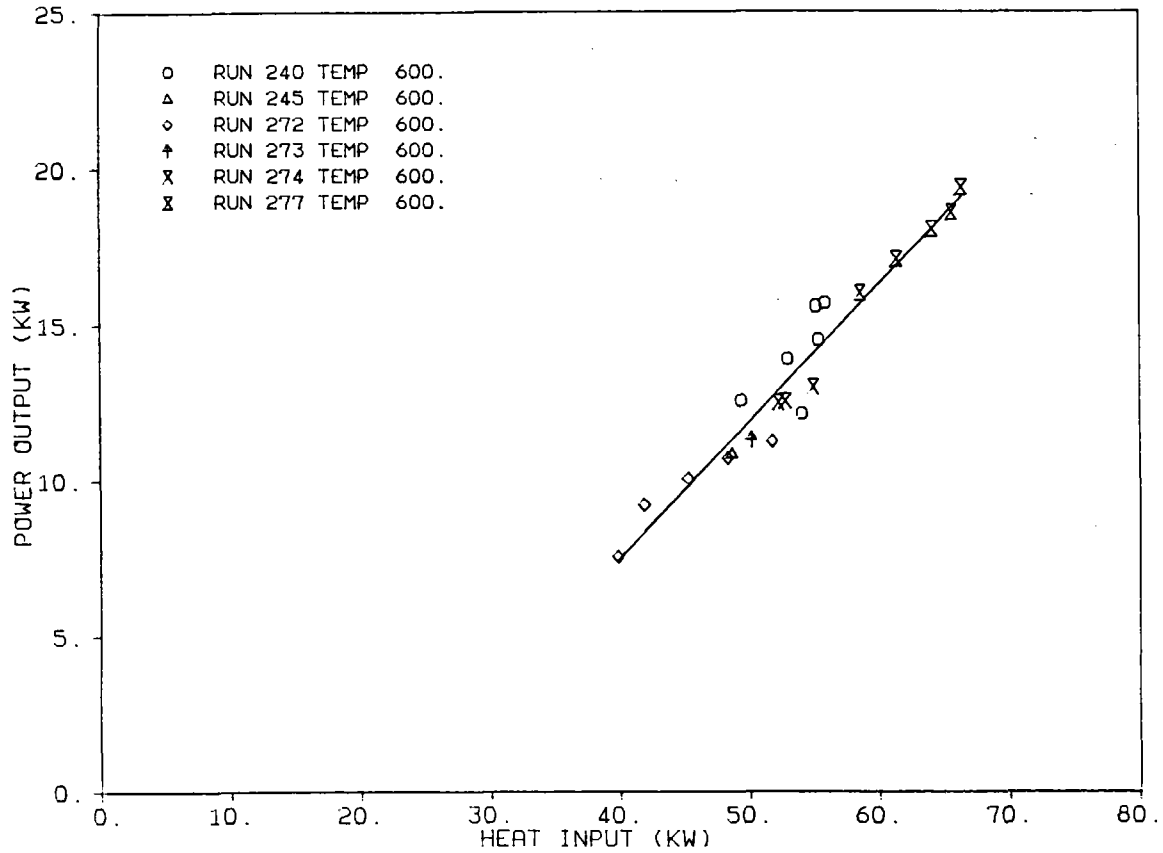

NDEG,SIGFAC 1 .8252

P = .00000000 1.00000000 -10.18243647 .44096844

RUN	X	Y	YFIT	R
240	54.100	12.1	13.674	-1.524
240	55.420	14.5	14.256	.264
240	55.880	15.7	14.459	1.231
240	55.190	15.6	14.155	1.425
240	53.020	13.9	13.198	.702
240	49.380	12.6	11.593	.967
245	48.690	10.8	11.288	-.448
272	41.950	9.2	8.316	.898
272	45.360	10.0	9.820	.230
272	48.380	10.7	11.152	-.432
272	51.780	11.2	12.651	-1.411
272	39.900	7.5	7.412	.118
273	50.230	11.3	11.967	-.657
274	55.030	13.0	14.084	-1.064
274	52.860	12.5	13.127	-.587
274	52.320	12.5	12.889	-.379
277	58.630	16.0	15.672	.328
277	61.340	17.1	16.867	.233
277	64.050	18.1	18.062	-.002
277	65.600	18.6	18.745	-.175
277	66.370	19.4	19.085	.285

ESOR-III, He, full
radiator, no window
T = 600°C
Z = 482 mm

Figure 6-18. Power Output versus Heat Input for ESOR-III (600°C, Z = 482 mm)

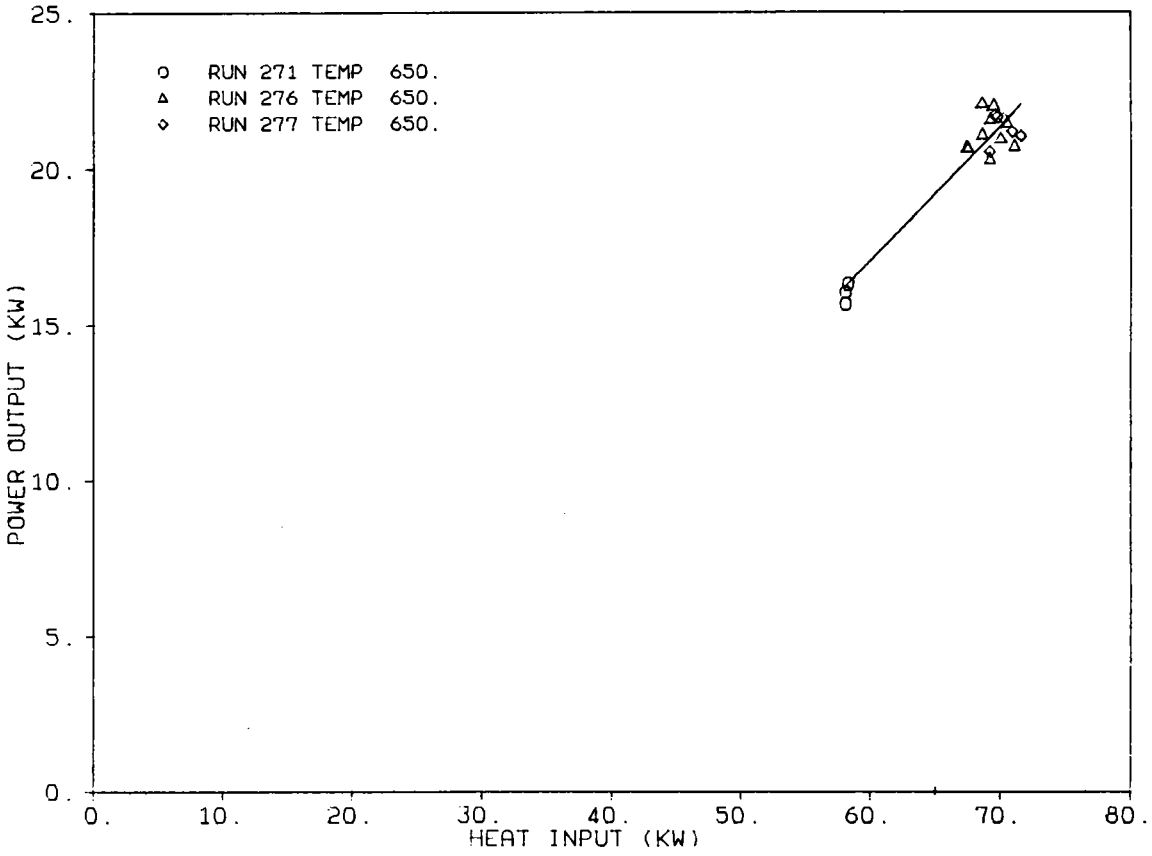

NDEG,SIGFAC 1 .6712

P = .00000000 1.00000000 -8.91131425 .43204059

RUN	X	Y	YFIT	R
271	58.130	16.0	16.203	-.183
271	58.280	16.3	16.268	.032
271	58.130	15.7	16.203	-.543
276	70.050	20.9	21.353	-.413
276	71.110	20.7	21.811	-1.101
276	70.530	21.4	21.561	-.131
276	69.180	20.3	20.977	-.697
276	68.600	21.1	20.727	.353
276	69.180	21.6	20.977	.593
276	69.470	22.0	21.103	.897
276	68.570	22.1	20.714	1.346
276	67.440	20.7	20.226	.434
276	67.530	20.7	20.264	.386
277	69.560	21.7	21.141	.539
277	69.760	21.6	21.228	.392
277	70.240	21.6	21.435	.135
277	70.920	21.2	21.729	-.579
277	71.600	21.0	22.023	-1.003
277	69.180	20.5	20.977	-.457

ESOR-III, He, full radiator, no window
T = 650°C
Z = 482 mm

Figure 6-19. Power Output versus Heat Input for ESOR-III (650°C, Z = 482 mm)

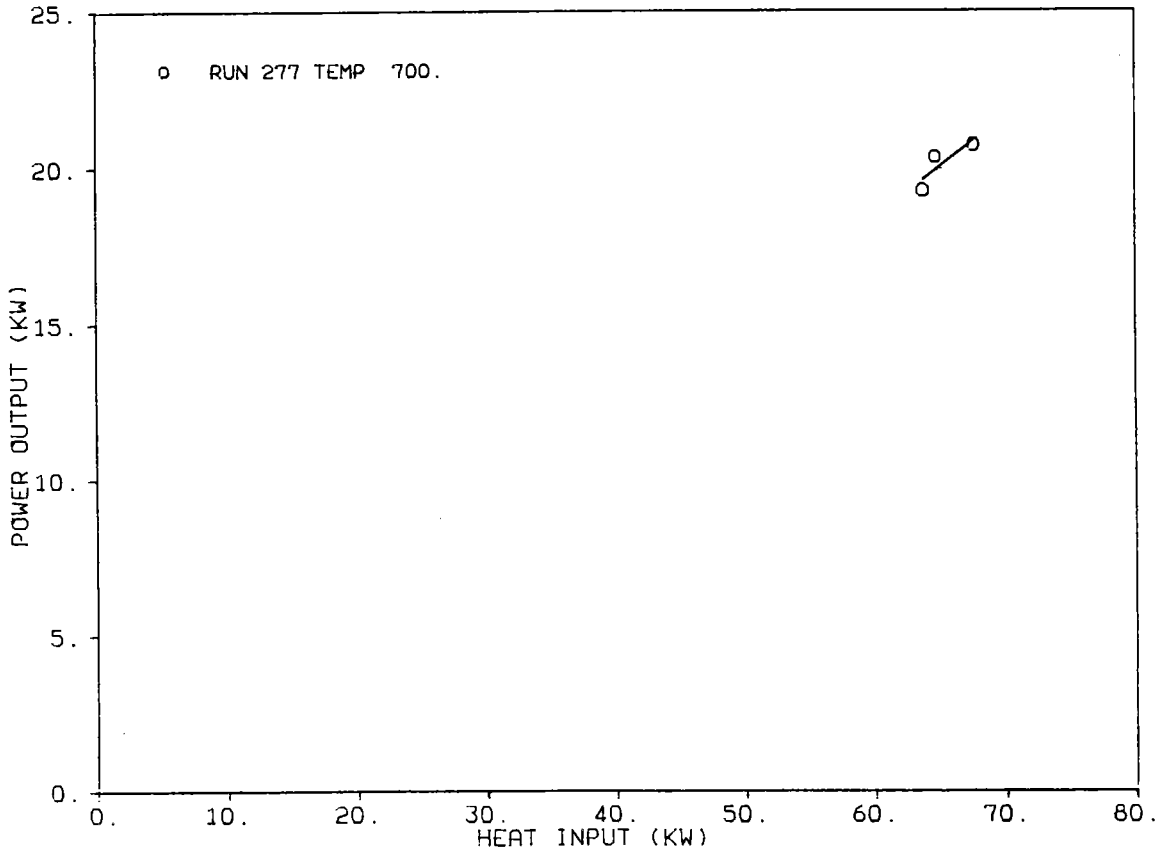

NDEG,SIGFAC 1 .5505

P = .00000000 1.00000000 -1.10663280 .32418876

RUN	X	Y	YFIT	R	
277	67.630	20.7	20.818	-.108	ESOR-III, He, full
277	64.730	20.3	19.878	.432	radiator, no window
277	63.760	19.2	19.564	-.324	T = 700°C
					Z = 482 mm

Figure 6-20. Power Output versus Heat Input for ESOR-III (700°C, Z = 482 mm)

Comparison of Figures 6-17 (hydrogen) and 6-20 (helium) provides information regarding the difference in power outputs resulting from the same configurations operating at 700°C and at the same, nearly full-load, heat power input but with the two different working fluids, hydrogen and helium. At Q_{in} = 65 kWt, $P_{out_{H_2}} - P_{out_{He}} = 0.9$ kWe. This is a much smaller difference than was established above in a similar comparison of configurations employing ESOR-IIB at 700°C; in that case $P_{out_{H_2}} - P_{out_{He}} > 2.5$ kWe was established. The very limited data available in Figure 6-20 and its accompanying table make the comparison of the ESOR-III configurations much less reliable than that of the ESOR-IIB configurations.

Figures 6-18 through 6-20 allow determination of the effect of heater head average gas temperature on the TBC-2/ESOR-III/USAB 4-95 (helium) configuration. Because of the previously mentioned limited data for the configuration operating at 700°C and the disparity in dP_{out}/dQ_{in} determined for Figure 6-20, the comparison will be made at Q_{in} = 65 kWt. Thus, P_{out} (650°C) - P_{out} (600°C) ≈ 0.75 kWe, while P_{out} (700°C) - P_{out} (600°C) ≈ 1.5 kWe. The reader should note that this difference in P_{out} due to the 100°C difference in heater head average gas temperature is comparable to those determined for configurations employing ESOR-IIA with or without a window in the receiver cavity, all tests having been conducted with helium as the working fluid. The usual cautions regarding the accuracy of these data should be recalled again in this consideration of tests involving ESOR-III.

G. ESOR-IV WITH HYDROGEN (CATEGORY NO. 7)

Figures 6-21 and 6-22 and their accompanying tables present test results for the TBC-2/ESOR-IV/USAB 4-95 (hydrogen) configuration operating at 600 and 650°C heater head average gas temperature, respectively. Obviously, the data are fragmentary; thus, the slopes and intercepts of the linear LSBF curves must be regarded as crude approximations. About all that can be gleaned from these two figures alone is that P_{out} (650°C) - P_{out} (600°C) ≈ 0.6 kWe at Q_{in} = 65 kWt.

H. ESOR-IV WITH HELIUM (CATEGORY NO. 8)

Figures 6-23 through 6-25 and their accompanying tables present test results for the TBC-2/ESOR-IV/USAB 4-95 (helium) configuration operating at 550, 600, and 650°C heater head average gas temperatures, respectively. The data at 600 and 650°C span a range of heat power input that provides plausible values of slope and intercept for the corresponding linear LSBF curves. From Figures 6-24 and 6-25, P_{out} (650°C) - P_{out} (600°C) ≈ 0.8 kWe, a value consistent with earlier results for other configurations operating under similar conditions. From Figures 6-23 and 6-25, P_{out} (600°C) - P_{out} (550°C) ≈ 1.1 kWe; this result appears reasonable, but the limited data employed in Figure 6-23 impose a correspondingly large uncertainty on this result.

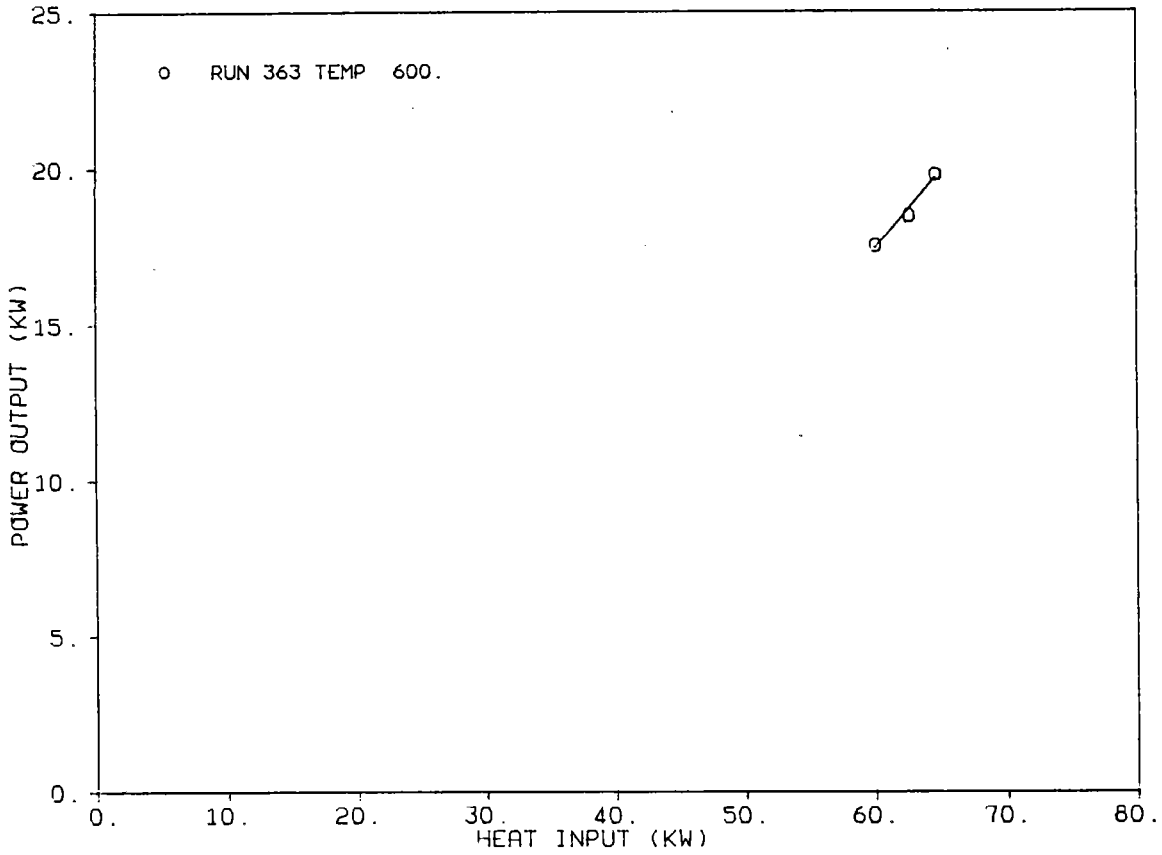

NDEG,SIGFAC 1 .2571

P = .00000000 1.00000000 -12.45576751 .49704913

RUN	X	Y	YFIT	R	
363	60.100	17.5	17.417	.093	ESOR-IV, H_2, full radiator,
363	62.600	18.5	18.660	-.210	no window
363	64.600	19.8	19.654	.116	T = 600°C

Figure 6-21. Power Output versus Heat Input for ESOR-IV with Hydrogen (600°C)

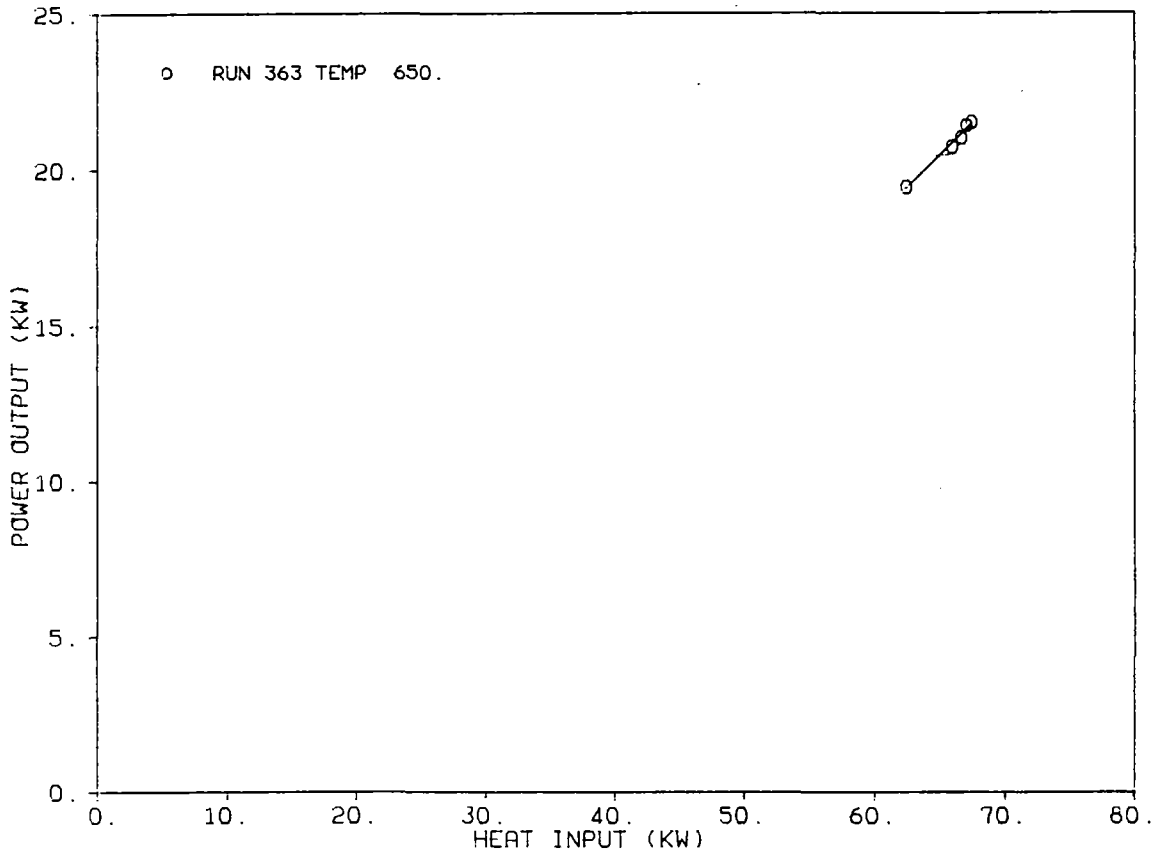

NDEG,SIGFAC 1 .1202

P = .00000000 1.00000000 -6.36901546 .41264828

RUN	X	Y	YFIT	R
363	62.400	19.4	19.380	.040
363	65.900	20.7	20.825	-.105
363	66.600	21.0	21.113	-.113
363	67.000	21.4	21.278	.122
363	67.400	21.5	21.443	.057

ESOR-IV, H_2, full radiator,
no window
T = 650°C

Figure 6-22. Power Output versus Heat Input for ESOR-IV with Hydrogen (650°C)

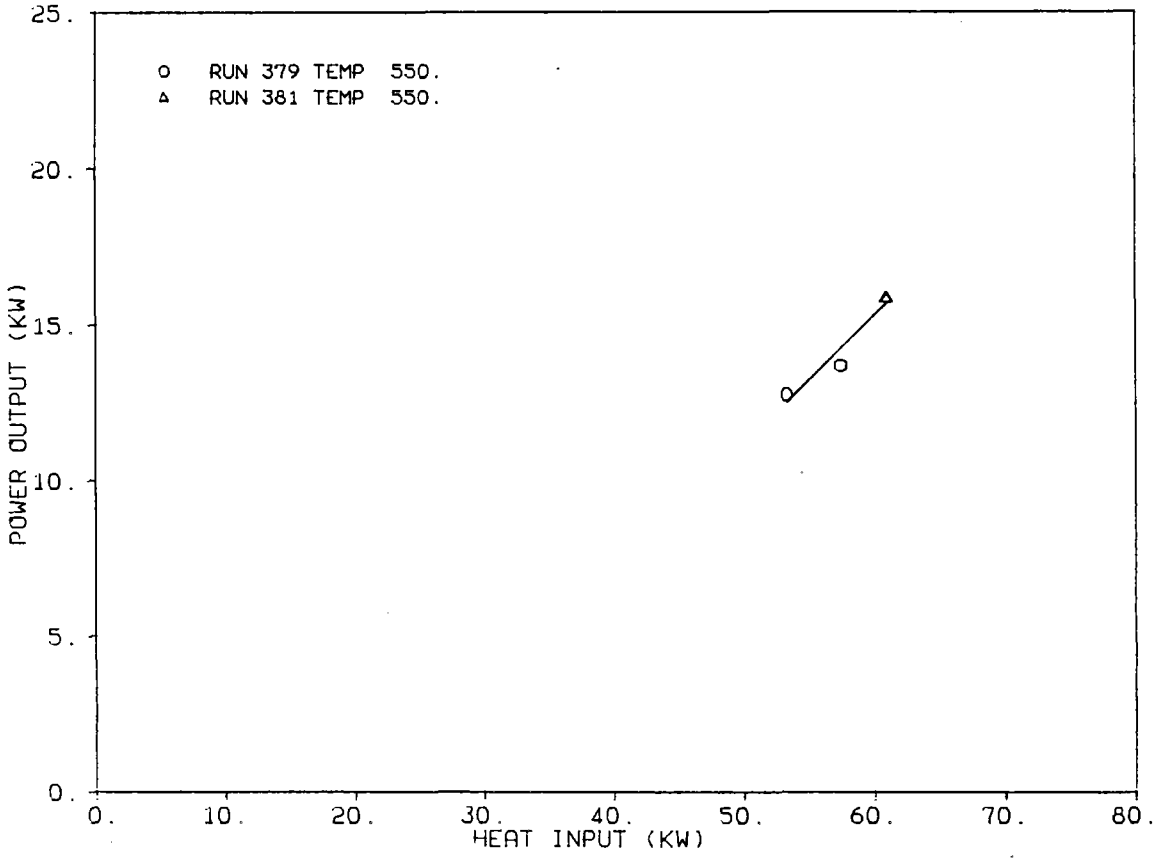

NDEG,SIGFAC 1 .4581

P = .00000000 1.00000000 -9.74623704 .41730383

RUN	X	Y	YFIT	R
379	54.470	13.7	14.236	-.556
379	53.300	12.7	12.496	.254
381	61.000	15.9	15.709	.141
381	60.950	15.9	15.688	.162

TBC-2
ESOR-IV, He, full radiator,
no window
T = 550°C
Z = 482 mm

Figure 6-23. Power Output versus Heat Input for ESOR-IV (550°C, Z = 482 mm)

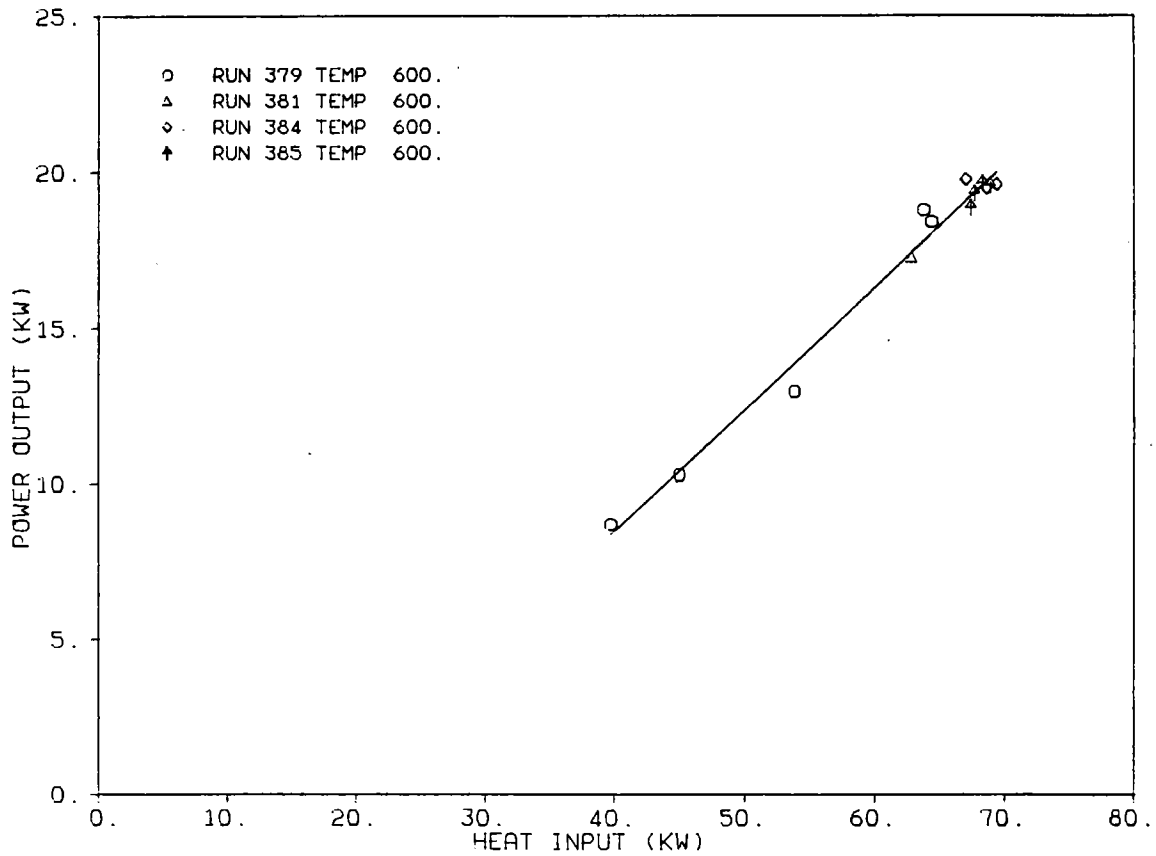

NDEG,SIGFAC 1 .5187

P = .00000000 1.00000000 -7.23721784 .39234705

RUN	X	Y	YFIT	R
379	39.760	8.7	8.363	.317
379	44.980	10.3	10.411	-.111
379	53.790	13.0	13.867	-.887
381	63.760	18.8	17.779	.991
381	64.340	18.4	18.006	.394
381	62.790	17.2	17.398	-.148
384	69.370	19.6	19.980	-.400
384	68.590	19.5	19.674	-.214
384	67.050	19.8	19.070	.690
385	68.890	19.5	19.792	-.262
385	67.720	19.3	19.333	-.053
385	67.430	18.8	19.219	-.379
385	68.300	19.6	19.560	.060

TBC-2
ESOR-IV, He, full radiator, no window
T = 600°C
Z = 457 mm on run 385
Others, Z = 482 mm

Figure 6-24. Power Output versus Heat Input for ESOR-IV (600°C, Z = 482 mm)

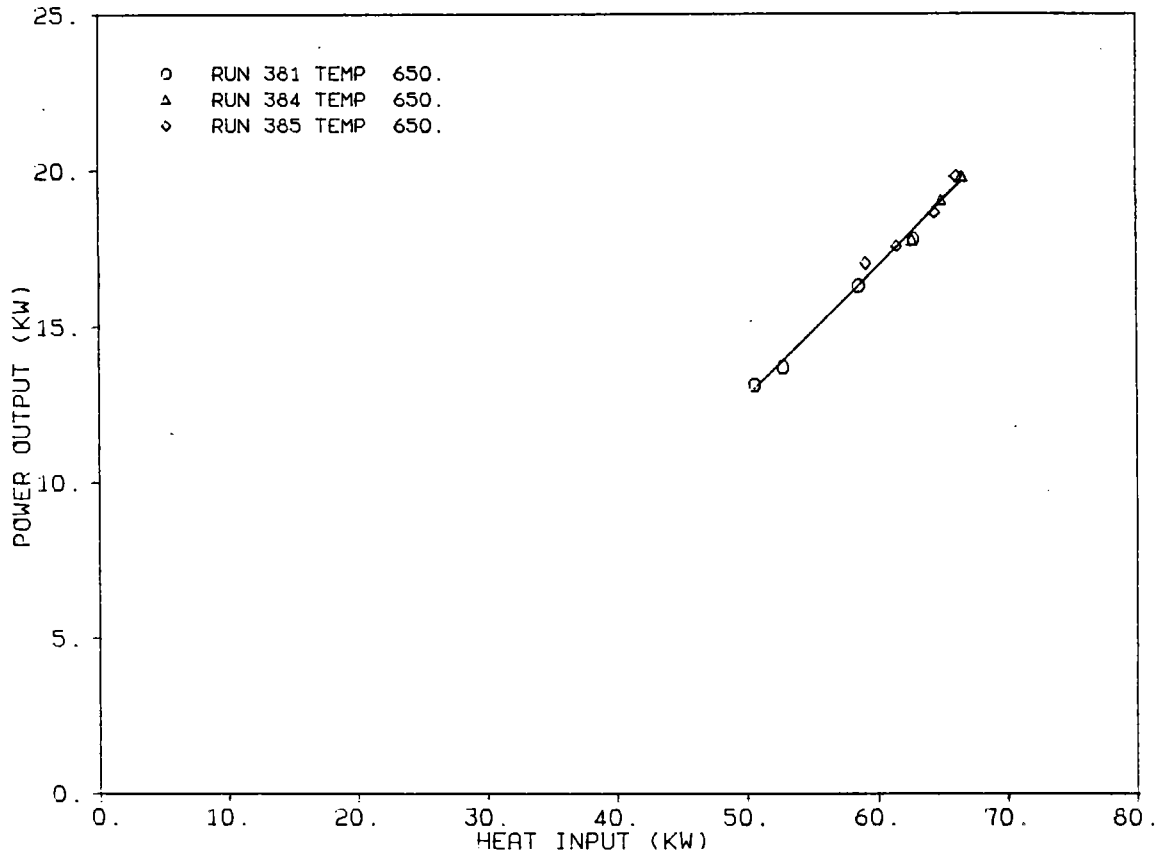

NDEG, SIGFAC 1 .2492

P = .00000000 1.00000000 -8.17395806 .41825845

RUN	X	Y	YFIT	R
381	50.600	13.1	12.990	.140
381	52.830	13.7	13.923	-.223
381	58.540	16.3	16.311	-.021
381	62.790	17.8	18.088	-.298
384	62.690	17.7	18.047	-.297
384	65.020	19.0	19.021	-.001
384	66.560	19.8	19.665	.095
385	59.100	17.0	16.545	.455
385	61.500	17.6	17.549	.011
385	64.440	18.6	18.779	-.139
385	66.170	19.8	19.502	.278

TBC-2
ESOR-IV, He, full radiator,
no window
1 = 650°C
Z = 482 mm
Z = 472 mm for run 385

Figure 6-25. Power Output versus Heat Input for ESOR-IV (650°C, Z = 482 mm)

Comparison of Figures 6-22 (hydrogen) and 6-25 (helium) allows another assessment of the performance improvement that can be expected from substituting hydrogen for helium in otherwise identical configurations at 650°C heater head average gas temperature:

$$P_{out_{H_2}} - P_{out_{He}} \approx 1.4 \text{ kWe}$$

Comparison of this with earlier results shows it to be intermediate to the differences exhibited by configurations employing ESOR-IIB (2.5 kWe) and ESOR-III (0.9 kWe) operating at 700°C when hydrogen was substituted for helium. It is unclear whether these variations in power output differences ascribed to changing the working gas are due to the possibly different receiver characteristics of the different module configurations or simply to uncontrolled differences in the test conditions under which only limited data were collected.

SECTION VII

TEST DATA INTERPRETATION

As a result of the paucity of module performance data under part-load conditions, it has been impossible, in those experiments where the thermodynamic medium was helium, to establish a well defined relationship between alternator power out, P_{out}, and solar power into the receiver aperture, Q_{in}. However, several early all-day tests were conducted on modules which employed hydrogen as the thermodynamic medium. These tests have allowed the slope of P_{out} versus Q_{in} to be established for the cases where hydrogen was employed as the engine working fluid. Thus,

$$0.44 < \left(\frac{dP_{out}}{dQ_{in}}\right)_{H_2} < 0.47.$$

As indicated above, it has proved impossible to establish a reasonably accurate corresponding $\left(\frac{dP_{out}}{dQ_{in}}\right)_{He}$ from module test data; therefore, another approach to the problem was required.

When the module test is conducted on a given concentrator in a given condition of cleanliness and with a fixed percentage of mirrors uncovered, the fraction of incident solar energy lost as a result of various concentrator imperfections is a constant. When receiver heater head gas mean temperature is held constant, receiver losses are, to a close approximation, also constant, independent of the load. Although, in the engine as in the receiver, there are secondary variable losses that are neither constant nor linear functions of the fractional load on the engine. When the engine and its accessories are operated at constant speed under varying load, the significant losses are either directly proportional to the load or are constant. Finally, the same constant loss component is present in a properly designed alternator operating at constant speed and at or below rated load; the chief contributors to this constant loss component are windage and bearing frictional losses. Because all the losses from the receiver and all losses from the engine and alternator not directly proportional to load are constant, the slope of the P_{out} versus Q_{in} equation is virtually constant and equal to the slope of the $P_{out} = P_{out_{alt}}$ versus $Q_{in_{eng}}$. The latter slope is, of course equal to the product

$$\left(\frac{P_{out}}{P_{in}}\right)_{alt} \cdot \left(\frac{P_{out}}{Q_{in}}\right)_{eng}$$

Nelving and Percival (Reference 3) presented a paper entitled "Modifications and Testing of a 4-95 Stirling Engine for Solar Applications." This

paper included a presentation of engine/alternator performance when the engine was charged with helium and operated at 720°C average heater head temperature, 50°C average cooling water temperature, and 1500 rev/min. This information led to the formula, $P_{out} = -4.64 + 0.462\ Q_{in}$, for the engine alternator assembly. Further review and analysis of the information available in References 1 and 2 led to the conclusion that, to the accuracy of the information available, the full-load efficiency of the power conversion assembly does not vary appreciably with engine rotational speed in the range $1500 \leq$ rev/min ≤ 1800. Technical considerations indicate that, at constant heater head mean gas temperature, the zero-heat-input power requirement of the engine/alternator combination should increase with rotational speed raised to approximately three-halves power; however, because full-load power is unaffected by rotational speed changes in the range of interest, it is inferred that compensating improvements in engine and or alternator performance must be occurring and the dP_{out}/dQ_{in} must increase as rotational speed increases.

In view of the limited data available and the limited accuracy of those data, it is believed the formula cited above and applicable at 1500 rev/min should also be considered valid at 1800 rev/min until more accurate, directly applicable results are available.

The data presented in the preceding discussions do not allow a more precise inference of dP_{out}/dQ_{in} in the case of either hydrogen or helium as the working medium. In fact, the choice of the same slope in either case appears to be warranted. Because of the limited number of data available for each of the many configurations and sets of conditions tested and because of the very limited number of data available at less than 80% of full load, even approximate estimates of the thermal power input required at zero alternator output power or of the negative power output required for zero thermal input power must be viewed as tentative. Still, within the range in which data are available, it has been possible to infer some definite conclusions.

A few early tests were conducted with the TBC-2/ESOR-IIA/USAB 4-95 (hydrogen) module configuration; however, the data from these tests were limited in number and suspect in accuracy. Because other receivers were more thoroughly tested with (1) pure hydrogen and (2) pure helium as the working fluid, only tests employing helium as the working fluid have been reported here for configurations that included ESOR-IIA. In contrast to the limited, early testing accomplished with configurations that included ESOR-IIA and employed hydrogen as a working fluid, by far the most extensive testing (involving the most varied configuration) was accomplished with ESOR-IIA and with helium as the working fluid. Results obtained from these tests have been reported in preceding paragraphs and figures.

An early series of tests involved testing the TBC-2/ESOR-IIA/USAB 4-95 (helium) configuration with the heater tube-cylinder head junctures set at various distances from the reference plane at the interface between the PCA mounting ring and mating face of the receiver. In these tests, the mirrored facets of the concentrator were defocused (1) to form an approximate ellipsoid of revolution of maximum flux on the axis of the concentrator and approximately centered on the mounting ring reference plane and (2) to direct the radiant flux away from the central plug within the receiver and onto

surrounding heater tubes. As seen from Figures 6-1 through 6-6 and the corresponding tables (spanning Z-distances from 457 mm to 582 mm), the effect of varying the axial distance from the aperture to the heater head had no significant effect on module performance at a constant average working gas temperature of 650°C within the heater heads. However, varying this distance did allow a shallow optimum to be established on the basis of uniformity of flux distribution and heater tube temperatures. The distance selected as optimum for following tests on any one of the receivers was virtually always 482, 507, or 532 mm.

SECTION VIII

STIRLING RECEIVER, ENGINE, AND ALTERNATOR EFFICIENCIES

The Stirling power module consists of a parabolic dish-type concentrator, a receiver into which concentrated solar rays are directed, a USAB 4-95 Stirling engine, and an induction-type alternator. A portion of the 60-Hz alternating current power generated is consumed in driving the radiator fan and water pump that are used to circulate the engine coolant. The remainder of this power is processed (i.e., voltage and power factor are corrected) and then supplied to the Southern California Edison Company's utility grid. In what follows, the net power delivered to the grid is defined as line power, whereas the gross output of the alternator is defined as the alternator power. This flow of power is shown in Figure 8-1.

Throughout this report, alternator power (gross output) has been reported and plotted against receiver input. In Section VI.E, the effect of change of radiator and water pump position and size was discussed. However, a firm set of parasitic power data is not available. As discussed in Section VI.E, attempts to reduce the parasitic power to between 1 and 1.5 kWe have not been conclusively demonstrated.[3]

Minimum and maximum values of the combined efficiency ($\eta_{rec} \cdot \eta_{eng} \cdot \eta_{alt}$) for the eight test categories discussed earlier are presented in Table 8-1.

Basic energy exchange rates for the Stirling power module are described below.

A. SOLAR INPUT INTO THE MODULE

Solar input into the module is defined as:

$$Q_{sol,in} = A_c \cdot I_b \qquad (1)$$

where A_c is the net projected concentrator mirror area and I_b is the beam of insolation.

The net projected mirror area exclusive of tabs, rods, receiver bipod, receiver aperture shutter, receiver ring and junction box shadows, and mirror speckles has been reported[4] to be 84.35 m^2. In an earlier study, the net area of the TBC with the original smaller ring area was calculated[5] to be 87.6 m^2. The difference between the original smaller ring area and the larger ring area is 0.43 m^2. Excluding this difference and the estimated

---

[3]Please see Footnote 2 on page 6-20.

[4]Dennison, E.W., JPL Internal Communication 353-081-228, April 28, 1982.

[5]Jaffe, L.D., JPL Internal Communication 316-1-006, March 19, 1982.

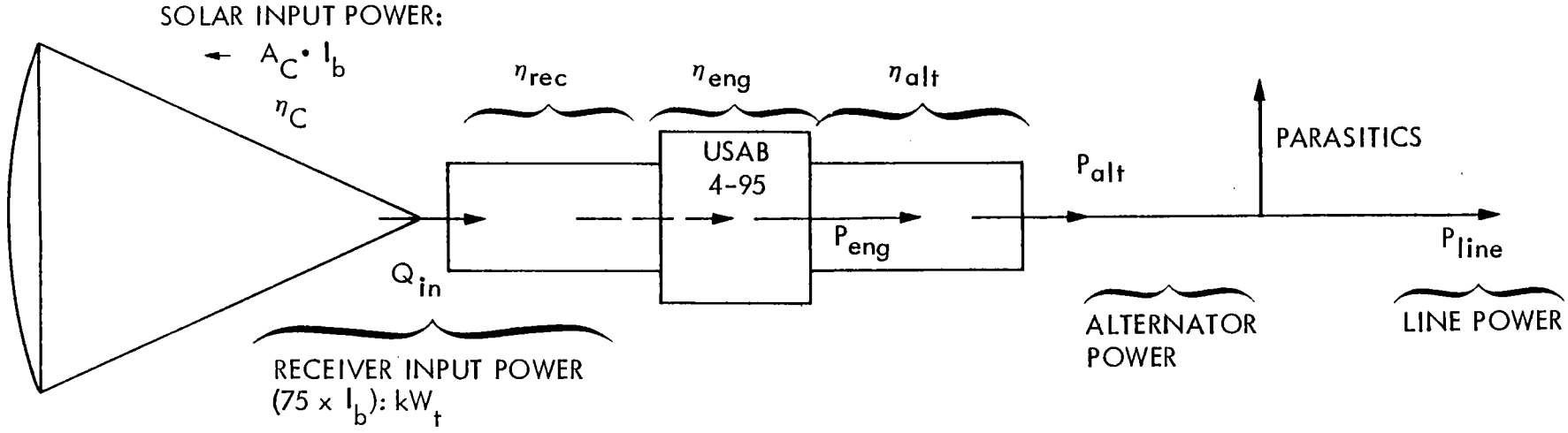

Figure 8-1. Energy Exchange and Efficiency of Stirling Module Components

Table 8-1. ESOR Efficiency Tests ($P_{alt}/Q_{in} = \eta_{comb}$)

Category	Figure	Run No.	ESOR	Working Fluid	Efficiency				Mean Heater Head Gas Temperature, °C	Conditions	η_{module}[b]	
					Min	% Load[a]	Max	% Load[a]			Min.	Max.
1	6-1	186,199,200	IIA	He	0.264	72.8	0.283	77.2	650	No Window Full Radiator	0.235	0.252
	6-2	183,196,197, 258,260,263	IIA	He	0.259	65.3	0.278	75.	650	"	0.231	0.247
	6-3	182,195	IIA	He	0.268	69.2	0.284	73.3	650	"	0.238	0.253
	6-4	180,181,190 192	IIA	He	0.225	61.3	0.286	74.6	650	"	0.2	0.254
	6-5	178,179	IIA	He	0.276	69.5	0.297	90.3	650	"	0.246	0.264
	6-6	177	IIA	He	0.263	92.9	0.28	94.1	650	"	0.234	0.249
	6-7	183,196,197, 198,260,261	IIA	He	0.192	43.0	0.29	85.7	650	"	0.17	0.258
	6-8	183,196,197, 258,260,263	IIA	He	0.259	65.5	0.282	74.9	650	"	0.23	0.25
	6-9	183,197,257, 258,260,261 263,264	IIA	He	0.258	68.7	0.286	88.8	700	"	0.229	0.254
	6-10	288,289,318	IIA	He	0.235	73.2	0.334	93.	600	"	0.209	0.297
	6-11	289,318	IIA	He	0.26	74.3	0.343	94.5	650	"	0.23	0.305
	6-12	289,318	IIA	He	0.26	70.9	0.325	97.7	700	"	0.23	0.301

[a] Based on 75 kW_t input at full load.

[b] Based on $\eta_{module} = \eta_{comb} \cdot \eta_{conc}$ and $\eta_{conc} = 0.89$.

Table 8-1. ESOR Efficiency Tests (Continued)

Category	Figure	Run No.	ESOR	Working Fluid	Efficiency Min	Efficiency % Load[a]	Efficiency Max	Efficiency % Load[a]	Mean Heater Head Gas Temperature,°C	Conditions	η_{module}[b] Min	η_{module}[b] Max
2	6-13	210,212	IIB	He	0.218	56.2	0.247	65.7	700	No Window Full Radiator	0.194	0.22
3	6-14	250,252,253, 265,266	IIA	He	0.228	69.6	0.277	90.6	700	With Window Full Radiator	0.21	0.246
	6-15	250,252,253, 255,265,266 268	IIA	He	0.247	66.8	0.291	89.3	700	With Window Full Radiator	0.22	0.259
4	6-16	324 338	IIA	He	0.26	80.8	0.283	96.7	700	No Window Variable Radiator	0.231	0.252
5	6-17	330	III	H_2	0.188	37.5	0.319	90.5	700	No Window Full Radiator (some partial load data)	0.167	0.284
6	6-18	240 ... 277			0.188	53.2	0.292	88.4	600	No Window Full Radiator	0.167	0.26
	6-19	271 ... 277	III	He	0.27	77.6	0.31	91.0	650	"	0.24	0.276
	6-20	277			0.31	86.3	0.313	90.1	700	"	0.276	0.278
7	6-21	363	IV	H_2	0.291	80.1	0.306	86.1	600	No Window	0.259	0.272
	6-22	363			0.31	83.6	0.319	89.9	650	Full Radiator	0.276	0.284
8	6-23	379,381	IV	He	0.252	71.0	0.261	81.3	550	No Window	0.225	0.232
	6-24	379 ... 385			0.219	52.9	0.284	92.0	600	Full Radiator	0.195	0.253
	6-25	381,384,385			0.259	67.4	0.299	88.6	650		0.23	0.266

total area of speckles (0.84 m^2), the correction amounts to 0.43 + 0.84 = 1.27 m^2. Thus corrected, the latter estimate becomes 86.33 m^2. There is still a difference of about 2.0 m^2 in net area definitions between the two estimates. Because the former estimate is more recent and includes details, the net area for the analysis herein has been accepted as 84.3 m^2.

Calorimetric measurements corrected to a 1.00-kW/m^2 insolation level have yielded a concentrated energy at the focal region of 75 kWt. This value has been used throughout this report. Thus, the concentrator efficiency can be obtained from the following equation:

$$\eta_C = 75/Q_{sol,in} = 75/84.3 = 0.89 \quad (2)$$

B. SOLAR INPUT INTO THE RECEIVER

As previously mentioned, the solar input into the receiver has been determined to be 75 $\pm$1.0 kWt at a nominal insolation level of 1.00 kW/m^2.

C. HEAT INPUT INTO THE ENGINE

Unfortunately, there have been no attempts to measure directly the rate of thermal energy input to the engine. If the efficiency of an identical mock-up receiver operating at the same temperature could have been experimentally determined, the heat input into the engine could have been obtained from:

$$Q_{in,eng} = 75 \cdot \eta_{rec} \quad (3)$$

Because such tests were not run, only the efficiency of the combined receiver-engine-alternator is analyzed here. This combined efficiency is defined as:

$$\eta_{combin} = \eta_{rec} \cdot \eta_{eng} \cdot \eta_{alt} \quad (4)$$

JPL has made no attempt to predict accurately the efficiency of the USAB-designed receiver assembly analytically. However, some effort has been made to calculate the efficiency of a generically similar receiver. A first attempt at such a calculation yielded an efficiency of 90% for a receiver operating at 870°C (Reference 4). Another attempt yielded an efficiency estimate for a well insulated receiver operating at 870°C of about 91% (Reference 5). Typical η_{rec} values were 91, 93, and 94% for temperatures of 870, 760, and 650°C, respectively. Thus, a receiver efficiency of 0.9 $\pm$0.04 at an operating temperature of 870°C can be assumed with considerable confidence. The receiver tested at the PDTS was probably not as well insulated; therefore, an efficiency estimate of 0.88 $\pm$0.04 is probably more appropriate. It should be noted that these efficiency estimates do not include the effect of wind on the receiver aperture. A slight efficiency improvement can be expected at lower operating temperatures. The highest tube temperatures experienced during tests were around 800°C, and corresponding mean gas temperatures were around 720°C. The receiver and tube temperatures were assumed to be the same. Thus, the receiver temperatures were calculated by adding 80°C to the corresponding gas temperatures. Under these conditions,

the receiver efficiency could be assumed to vary from 89 to 91%, the higher value corresponding to the lower temperature.

D. ENGINE EFFICIENCY

Because the test configuration was not designed to measure the net heat power input to the engine and the net shaft power output, the efficiency must be derived from the combined efficiency data. Rearranging Equation 4 yields:

$$\eta_{eng} = \eta_{combin}/(\eta_{rec} \cdot \eta_{alt}) \quad (5)$$

The combined efficiency has been determined; ranges for this overall efficiency of the power conversion assembly are tabulated in Table 8-2. Data from all eight test categories are included in this table. Receiver efficiency values adopted were fitted to a linear curve:

$$\eta_{rec} = 0.98534 - 0.00010\ T_{rec} \quad (6)$$

where T_{rec} is receiver temperature in °C.

The alternator efficiency has been fitted to a parabolic curve based on USAB data from tests run in Sweden.[6]

$$\eta_{alt} = -0.0002203\ P^2 + 0.0037896\ P + 0.92192 \quad (7)$$

Using η_{combin} obtained from ESOR test data, the engine efficiency can be determined from Equation 5.

In Table 8-2, typical points from selected runs within each category have been used to determine the engine efficiency, and these results are compared with the curve-fitted results from tests run in Sweden. The data from tests run in Sweden, using helium and hydrogen as the working fluids, are presented in Figures 8-2 and 8-3.

The latter part of Table 8-2 gives the engine efficiency calculated by applying Equation 5 to PDTS test data.

Efficiency curves are given for 50°C coolant exit temperature (Figures 8-2 and 8-3). A 20°C increase of cooling water results in a reduction of engine efficiency of about 2.1 percentage points at T_H = 720°C. For T_H = 920°C the efficiency is reduced by 2 percentage points by a coolant exit temperature rise of 20°C. On the average, 1 percentage point per 10°C increase in coolant exit temperature can be assumed.

In the first half of Table 8-2, the engine efficiency is determined by using load (kWe), hot working gas temperature (T_H) in °C, and working gas pressure (P_{gas}) in MPa, and Figure 8-2 or 8-3. Because these curves are applicable to a coolant exit temperature of 50°C, additional correction was applied (as explained in the preceding paragraph) to obtain the engine efficiency based on USAB test curves. These values are given under the heading "@ T_C" in Table 8-2.

---

[6]Courtesy H. Nelving, USAB, Malmo, Sweden.

Table 8-2. Comparison of Stirling Subsystem Efficiencies

Category/ Figure	RUN No.	kW_e	T_H (°C)	Cool Outlet (T_C)	Based on USAB Tests in Sweden η_{eng} (from Figs. 8-2/3) @ T_C=50°C	Based on USAB Tests in Sweden η_{eng} (from Figs. 8-2/3) @ T_C[a]	Derived from PDTS Tests $T_{rec} = T_H + 80°C$ η_{combin}[b]	η_{rec}[c]	η_{alt}[d]	η_{eng}[e]	η_{module} (PDTS Data) $\eta_{module} = \eta_{combin} \cdot \eta_{conc}$[f]
1/ 6-1 He	186	15.4	652	70	0.334	0.313	0.279	0.92	0.9255	0.33	0.248
6-2 He	258	12.7	657	43	0.324	0.33	0.2836	0.92	0.929	0.331	0.23
6-3 He	195	15.2	658	60	0.335	0.325	0.2836	0.92	0.929	0.331	0.252
6-4 He	192	14.0	650	55	0.325	0.32	0.274	0.92	0.93	0.32	0.244
6-5 He	178	19.7	656	60	0.342	0.331	0.289	0.92	0.911	0.344	0.257
6-6 He	177	19.3	658	60	0.342	0.331	0.237	0.92	0.912	0.325	0.211
6-7 He	198	6.2	599	60	0.264	0.255	0.191	0.923	0.938	0.22	0.17
6-7 He	261	18.8	609	41	0.325	0.334	0.292	0.923	0.915	0.346	0.259
6-8 He	163	15.6	659	35	0.331	0.346	0.277	0.92	0.926	0.325	0.246
6-9 He	257	13.3	708	36	0.343	0.358	0.258	0.89	0.933	0.31	0.23
6-10 He	263	19.1	706	41	0.36	0.37	0.312	0.89	0.912	0.384	0.277
6-10 He	288	14.0	600	60	0.298	0.288	0.247	0.923	0.93	0.288	0.22
6-11 He	289	14.8	650	61	0.332	0.321	0.245	0.938	0.929	0.281	0.218
	318	22.2	650	54	0.345	0.341	0.314	0.938	0.893	0.375	0.279
6-12 He	289	14.7	700	63	0.35	0.337	0.272	0.91	0.929	0.322	0.242

[a] At coolant outlet temperature of T_C

[b] $\eta_{combin} = \eta_{eng} \cdot \eta_{rec} \cdot \eta_{alt}$

[c] $\eta_{rec} = 0.98534 - 0.0001\, T_{rec}$

[d] $\eta_{alt} = -0.0002203\, P_{kw}^2 + 0.0037896\, P_{kw} + 0.9219$

[e] $\eta_{eng} = \eta_{combin}/(\eta_{rec} \cdot \eta_{alt})$

[f] $\eta_{conc} = 0.89$

Table 8-2. Comparison of Stirling Subsystem Efficiencies (Cont'd)

Category/ Figure	RUN No.	kW_e	T_H (°C)	Cool Out-let (T_C)	Based on USAB Tests in Sweden η_{eng} (from Figs. 8-2/3) @ T_C=50°C	Based on USAB Tests in Sweden η_{eng} (from Figs. 8-2/3) @ T_C[a]	Derived from PDTS Tests $T_{rec} = T_H + 80°C$ η_{combin}[b]	η_{rec}[c]	η_{alt}[d]	η_{eng}[e]	η_{module} (PDTS Data) $\eta_{module} = \eta_{combin} \cdot \eta_{conc}$[f]
2/6-13 He	210	9.4	659	65	0.294	0.28	0.222	0.915	0.938	0.259	0.197
	212	12.2	699	65	0.335	0.32	0.245	0.905	0.937	0.29	0.218
3/6-14 He	252	11.9	600	36	0.296	0.31	0.228	0.923	0.935	0.264	0.203
	266	17.8	600	35	0.314	0.329	0.27	0.923	0.919	0.318	0.24
6-15 He	252	12.4	700	35	0.341	0.356	0.247	0.912	0.933	0.29	0.22
	268	19.5	700	35	0.36	0.375	0.298	0.912	0.911	0.357	0.265
4/6-16 He	326	15.6	669	50	0.335	0.335	0.26	0.924	0.926	0.307	0.23
	338	18.4	698	58	0.365	0.357	0.271	0.905	0.915	0.327	0.24
5/6-17 H_2	330	5.3	726	51	0.27	0.269	0.1885	0.885	0.939	0.227	0.168
	330	21.1	702	38	0.388	0.4	0.319	0.89	0.904	0.396	0.284
6/6-18 He	272	7.5	600	43	0.265	0.272	0.188	0.923	0.938	0.2171	0.167
	277	19.4	600	40	0.315	0.325	0.292	0.923	0.911	0.347	0.26
6-19 He	271	16.0	650	42	0.326	0.334	0.275	0.938	0.925	0.317	0.245
	277	21.6	650	41	0.34	0.349	0.307	0.938	0.91	0.36	0.273
6-20 He	277	20.7	700	45	0.365	0.37	0.30	0.91	0.91	0.362	0.267
7/6-21 H_2	363	19.8	600	25	0.343	0.368	0.306	0.923	0.910	0.364	0.272
6-22 H_2	363	21.5	650	29	0.366	0.387	0.319	0.938	0.91	0.374	0.284

Table 8-2. Comparison of Stirling Subsystem Efficiencies (Cont'd)

Category/ Figure	RUN No.	kW_e	T_H (°C)	Cool Outlet (T_C)	Based on USAB Tests in Sweden η_{eng} (from Figs. 8-2/3) @ T_C=50°C	Based on USAB Tests in Sweden η_{eng} (from Figs. 8-2/3) @ T_C[a]	Derived from PDTS Tests $T_{rec} = T_H + 80°C$ η_{combin}[b]	η_{rec}[c]	η_{alt}[d]	η_{eng}[e]	η_{module} (PDTS Data) $\eta_{module} = \eta_{combin} \cdot \eta_{conc}$[f]
8/6-23 He	381	15.9	500	22	0.245	0.273	0.26	0.94	0.926	0.299	0.231
6-24 He	379	8.7	607	24	0.275	0.301	0.219	0.92	0.938	0.253	0.195
	385	19.3	589	38	0.315	0.328	0.285	0.92	0.912	0.337	0.254
6-25 He	381	13.1	641	28	0.315	0.337	0.259	0.938	0.933	0.296	0.23
	384	19.0	648	30	0.335	0.355	0.292	0.938	0.912	0.341	0.26

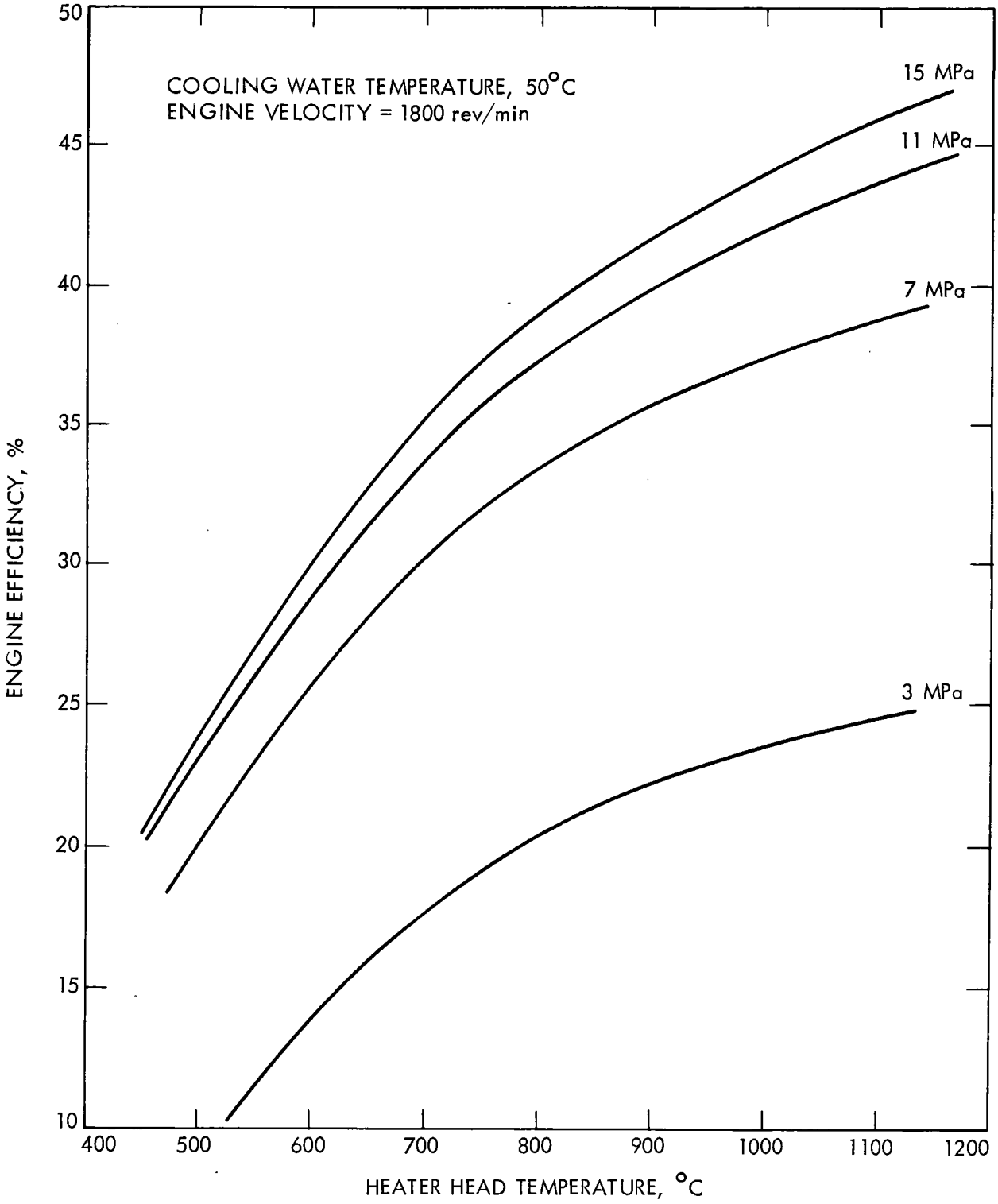

Figure 8-2. Stirling Engine Efficiency As a Function of Heater Temperature and Pressure with Helium as the Working Fluid (Courtesy USAB)

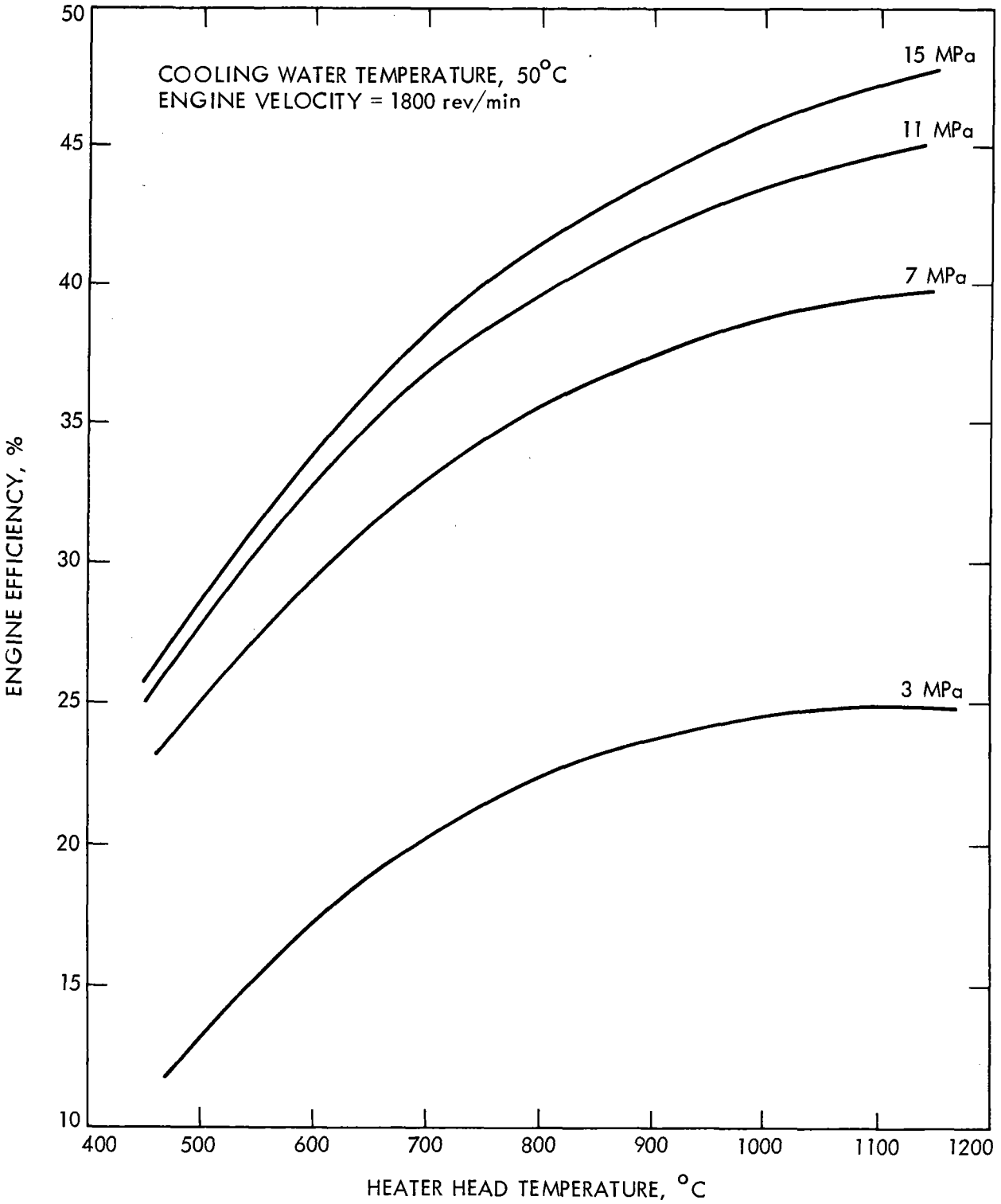

Figure 8-3. Stirling Engine Efficiency as a Function of Heater Temperature and Pressure with Hydrogen as the Working Fluid (Courtesy USAB)

Ultimately, the engine efficiency from the curves obtained from testing at USAB in Sweden compares reasonably well with the engine efficiencies calculated from PDTS test data. (See Based on USAB Tests in Sweden, η_{eng}, and Derived from PDTS Tests, η_{eng}, respectively, in Table 8-2.)

Tables 8-1 and 8-2 give module efficiencies based on a concentrator efficiency of 89% that corresponds to the output of a clean TBC. Module efficiency thus follows the trend of the receiver/engine/alternator combination efficiency. Module efficiency is a function of the percent load applied as well as the type of receiver, operating temperature, and working fluid.

Although test results reported throughout this report and in Table 8-1 vary considerably, a summary of findings are presented below to give an idea of ballpark values:

(1) ESOR-IIA with helium near full load (>90%) at 650°C mean heater head temperature yielded module efficiencies ranging from 0.234 to 0.305. At about three quarters load (70-80%), the efficiency ranged from 0.23 to 0.254.

(2) ESOR-IIB yielded module efficiencies ranging from 0.194 to 0.22 at 700°C near half load (56-65%).

(3) ESOR-III produced a module efficiency at 90% load using hydrogen as the working fluid of about 0.284. The same receiver yielded a module efficiency of about 0.278 when helium was used instead of hydrogen under similar conditions.

(4) ESOR-IV tests with hydrogen at 650°C yielded a module efficiency of about 0.284 at 90% load. Using helium instead of hydrogen reduced the module efficiency to 0.266 under similar conditions. At 600°C, hydrogen tests were run at loads ranging from 80 to 86%; these tests yielded module efficiencies ranging from 0.259 to 0.272.

When helium replaced hydrogen at 600°C near full load (92%), the module efficiency was reduced to 0.253. At partial load (53%) the module efficiency was further reduced to 0.195.

SECTION IX

CONCLUSIONS

The following conclusions are drawn from this independent analysis:

(1) The efficiency of the USAB 4-95 Stirling engine, as calculated by the author from PDTS test data, compares reasonably well with the efficiency values obtained by USAB from testing in Sweden. Because the receivers tested by USAB at the PDTS formed an integral part of the power conversion assembly (PCA) in every case, receiver efficiency could only be inferred by the author from analysis and from PCA performance experimentally established on the basis of PDTS engine/alternator data. Module efficiency can then be determined by taking into account the concentrator efficiency, which in this case is 89% for the TBC. Module efficiency ranged from 23.4 to 30.5%, depending upon the receiver type and working fluid (hydrogen or helium) near full load for temperatures from 650 to 700°C.

(2) The tests conducted by USAB provided them with extended operating experience with the USAB-supplied engine/receiver combinations in a test environment involving full-load or virtually full-load operation with a solar energy source. The data base for part-load operation developed during these tests is extremely limited.

(3) Following preliminary testing of ESOR-I, subsequent reconfiguration of the TBC mirrors, and determination of a near-optimum Z-axis position for the receiver aperture plane during testing of ESOR-IIA and B, no appreciable variation in PCA performance or efficiency was apparent in other configurations. Uniformity of heat flux on the Stirling engine heater head quadrants probably was progressively improved in later tests. Potential heater head life probably was extended by knowledge gained in this way; however, power conversion assembly performance and efficiency were not noticeably improved during these later tests.

(4) In every case, the installation of a quartz window in a receiver resulted in a slight reduction in the performance of the otherwise unchanged PCA.

(5) Independent tests of at least some of the receivers would have provided useful additional data from direct measurement of receiver performance.

(6) When operating at a PCA shaft speed of 1800 rev/min, an increase in heater head mean gas temperature from 600 to 700°C appears to increase the electric power output of the PCA by about 1.5 to 2.0 kWe when the heat power input to the receiver is 60 kWt. This increase in output appears to be about the same, whether the working fluid employed by the engine is helium or hydrogen.

(7) When operating at a PCA shaft speed of 1800 rev/min, a heater head temperature of 600 to 700°C, and 30 to 60 kWt heat power input to the receiver, the electrical power output of the PCA is about 1 to 2.5 kWe greater when the engine is charged with hydrogen than when the engine is charged with helium. Whether the wide variation observed in this effect is due to differences in configuration, inaccuracies in the test data, or both is not clear.

(8) An unusually high rate of coolant water flow with a correspondingly unusually low coolant temperature rise and, coincidentally, an unusually large coolant pumping power requirement were noted throughout the test program. Possible reasons why such a high flow rate was maintained have been mentioned in the body of the report, but no conclusions are drawn in this last respect.

(9) The extensive testing of partially covered radiator air flow passages indicates that the radiator core area could probably be reduced by about one half without serious effect on module performance. However, no conclusion is possible regarding how much air cooling fan and water pump parasitic power might be reduced by proper cooling system optimization.

SECTION X

REFERENCES

1. Kelm, G.G., Cairelli, J.E., and Walter, R.J., "Test Results and Facility Description for a 40-Kilowatt Stirling Engine," DOE/NASA/51040-27, June 1981.

2. Kelm, G.G., Cairelli, J.E., and Tew, Jr., R.C., "Performance Sensitivity of the P40 Stirling Engine," presented at the Automotive Technology Development Contractor Coordination Meeting, Dearborn, Michigan, October 26-29, 1981.

3. Nelving, H.G., and Percival, W.H., "Modifications and Testing of a 4-95 Stirling Engine for Solar Applications," Parabolic Dish Solar Thermal Power Annual Program Review Proceedings, JPL Publication 82-66, DOE/JPL-1060-52, Jet Propulsion Laboratory, Pasadena, California, July 15, 1982.

4. Fujita, T., Bowyer, J., and Gajanana, B., "Comparison of Advanced Engines for Parabolic Dish Solar Thermal Power Plants," 15th Intersociety Energy Conversion Engineering Conference, Seattle, Washington, August 1980; J. of Energy, Vol. 6, No. 5, pp. 293-297, September-October 1982.

5. Selcuk, M.K., and Fujita, T., A Nomographic Methodology for Use in Performance Trade-Off Studies of Parabolic Dish Solar Power Modules, JPL Publication 84-39, DOE/JPL-1060-74, Jet Propulsion Laboratory, Pasadena, California, June 15,1984.